THE ANALYSIS OF ANGULAR CORRELATIONS OF RADIATIVE TRANSITIONS AND AN INVESTIGATION OF EXCITED STATES OF Cl^{35}

by

Denny D. Watson
B.S., University of Kansas, 1960

Submitted to the department of Physics and Astronomy and the Faculty of the Graduate School of the University of Kansas in partial fulfillment of the requirements for the degree of Doctor of Philosophy.

Advisory Committee:

Redacted Signature

Chairman

Redacted Signature

Redacted Signature

TABLE OF CONTENTS

TABLE OF CONTENTS (Cont'd)

SECTION 1

Introduction to the Thesis

The original intent of this thesis problem was the experimental study of the Cl^{35} nucleus by the measurement and analysis of angular correlations and linear polarizations of gamma rays from the radiative capture of protons by S^{34}. The angular correlation data was originally analyzed using the numerical tables of Smith[1] to calculate the theoretical correlations, and using a graphical technique to compare the experimental results with the theoretical correlations. The complete analysis of this data by that system required the calculation of a number of additional coefficients which were not tabulated in Ref. 1. It also appeared that the graphical solutions, in one instance, were not sufficiently accurate to provide a unique spin assignment from the experimental data.

At this time a new formalism for the description of gamma-ray angular correlations became available[2]. A complete set of numerical coefficients was necessary before this formalism could be utilized. The new formalism, however, appeared to have such a great potential for a solution of the existing data analysis problems that the task of calculating and tabulating an extended set of coefficients was undertaken. The tabulation is too lengthy to include in this thesis and is being published under separate cover. Section 2 of the thesis is a part of the introduction to the numerical tabulation and it is included here since it provides a review of the formulae which have been used in the analysis of the Cl^{35} data.

The new formalism was next incorporated into a much more complete and precise data analysis system. The new data analysis techniques are discussed in Section 3. The implementation of these data analysis techniques requires a lengthy computer program. Such a program has been written and is discussed briefly in Appendix II. The length of the computer program prohibits the inclusion of a complete listing in the thesis and thus it, also, is being published in more detail under separate cover.

Some results of the experimental work are discussed in Sections 4 and 5. The applications of the formalism and the data analysis system are illustrated and the determination of some spins, parities, and mixing ratios from the $S^{34}(p,\gamma)$ work is reported. All of the experimental data has been analyzed independently by techniques which existed prior to the new developments discussed above. The results of both analyses are in good agreement. The results from the new system have been so much more accurate and easily communicated, however, that the original data analysis has not been discussed.

The author is fortunate to be now employed at a laboratory where a further investigation of the properties of Cl^{35} is being carried on by him and others in a professional capacity. The work described in this thesis serves as a foundation for a more comprehensive study.

---

1. P.B. Smith, in Nuclear Reactions, Vol II, edited by P. M. Endt and P. B. Smith, (North-Holland Publishing Company, Amsterdam, (1962)).

2. G.I. Harris, H.J. Hennecke, and D.D. Watson, "On the Analysis of Triple Correlation Measurements," to be published.

SECTION 2.

Angular Correlation Formalism

2.1 Introduction

Excellent treatments of the theory of angular correlations between gamma-rays in successive radiative transitions from isolated aligned nuclear states have been provided by Biedenharn and Rose[1], Rose[2], Satchler[3], Devons and Goldfarb[4], Litherland and Ferguson[5], and many others. The application of various forms of the theory to the numerical analysis of experimental data has been discussed by Ferguson and Rutledge[6], Smith[7,8], Ferguson[9], and others.

The formalism used by Ferguson and Rutledge involves both formation and decay parameters mixed into a single formula with no explicit reference to any magnetic substates. Litherland and Ferguson have developed the formalism beginning with an aligned but arbitrarily populated initial nuclear state. This replaces non-linear formation parameters by linear population or statistical tensor parameters and, in consequence, tends to simplify data analysis. Harris, Hennecke and Watson[10], hereafter referred to as HHW, have developed a formalism in its "factored" form in which the initial state is specified by population or tensor parameters in product with a separate factor representing each gamma-radiation of a gamma-decay cascade. This formalism is extended in a natural way to cover multiple cascades where any number of gamma-radiations are unobserved. The intrinsic factorization property can be useful in the

numerical analysis of data. In addition, the attendant numerical coefficients are more compact and thus more easily extended to cover a greater variety of problems. These coefficients have been tabulated under separate cover[11].

The tabulated coefficients allow the calculation of angular correlations of gamma-rays from a general n-step cascade where any one gamma-ray or any two gamma-rays in coincidence are observed. Coefficients for both the population parameter and statistical tensor formalism are tabulated. The gamma-ray multipolarities may be as high as octupole.

The next three sections contain a list of formulae from HHW which are relevant to the calculation of angular correlations. The coefficients involved in these formulae will be defined in section 2.5.

The notation used here is essentially the same as that used by HHW. Two exceptions must be noted. The ordering of quantum numbers $J_1LL'J_2$ is used here in place of J_1J_2LL' used in HHW, and also the small u and capital U have been interchanged. The latter change was adopted in order to provide notational symmetry between the u and h coefficients. The capital U of HHW was chosen to agree with the notation of references 2 and 3. Within the context of this work and that of HHW, this seemed to be the least confusing choice of notations. The phase convention in HHW and in this paper is the same as that used by Smith [7] and also by Ferguson and Rutledge[6] in the 1962 edition of their tables.

2.2 The Population Parameter Representation

2.2.1 Ordinary Triple Correlations

The ordinary triple correlation formula for a double cascade as shown in Fig. 2.1 is given by:

$$W(\Omega) = \sum_{m\,M} P_m(J_1)\, G_{mM}(\delta_1, \Omega)\, H_M(\delta_2) \,. \qquad (2\text{-}1)$$

Pm is the population of the + m and -m magnetic substates taken together. Ω stands for some set of the three angles θ_1, θ_2, ϕ which specify the angles of the first and second gamma-rays measured from the incoming beam axis and the aximuthal angle between the gamma-rays as shown in Fig. 2.2. The summation runs over all values of m and M for which the coefficients do not vanish. The other factors are given in terms of the tabulated coefficients as follows:

$$H_M(\delta_2) = \frac{h_M(J_2 L_2 L_2 J_3) + \delta_2\, h_M(J_2 L_2 L_2' J_3) + \delta_2^2\, h_M(J_2 L_2' L_2' J_3)}{1+\delta_2^2}$$

$$\equiv \sum_{L_2 L_2'} \frac{\delta_2^{p_2}}{1+\delta_2^2}\, h_M(J_2 L_2 L_2' J_3) \,. \qquad (2\text{-}2)$$

$$G_{mM}(\delta_1, \Omega) = \sum_{K\,N} \sum_{L_1 L_1'} \frac{\delta_1^{p_1}}{1+\delta_1^2}\, E^N_{KM}(J_1 L_1 L_1' J_2 m)\, Q_K\, Q_M\, X^N_{KM}(\Omega), \qquad (2\text{-}3)$$

where

$$X^N_{KM}(\Omega) \equiv X^N_{KM}(\theta_1, \theta_2, \phi)$$

$$= \left[\frac{(2M+1)(2K+1)(K-N)!\,(M-N)!}{(K+N)!\,(M+N)!}\right]^{1/2} P^N_K(\theta_1)\, P^N_M(\theta_2)\, \cos N\phi \,. \qquad (2\text{-}4)$$

The quantities δ_1 and δ_2 are the ratios of reduced matrix elements for L'-pole to L-pole radiation. The exponents p_1 and p_2 take on the values 0, 1, or 2 for pure L, mixed L, L', or pure L' radiation, respectively.

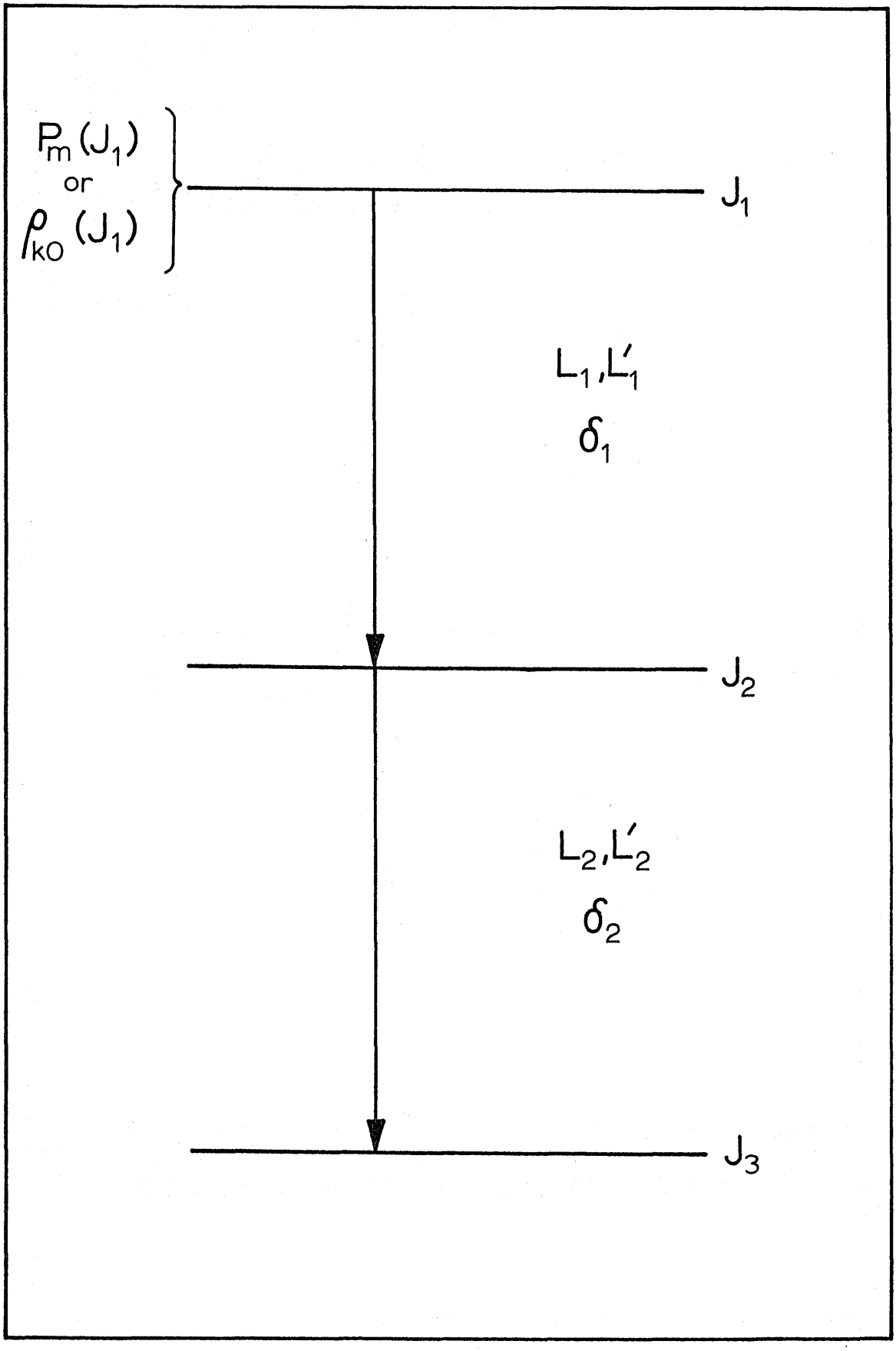

Fig. 2.1

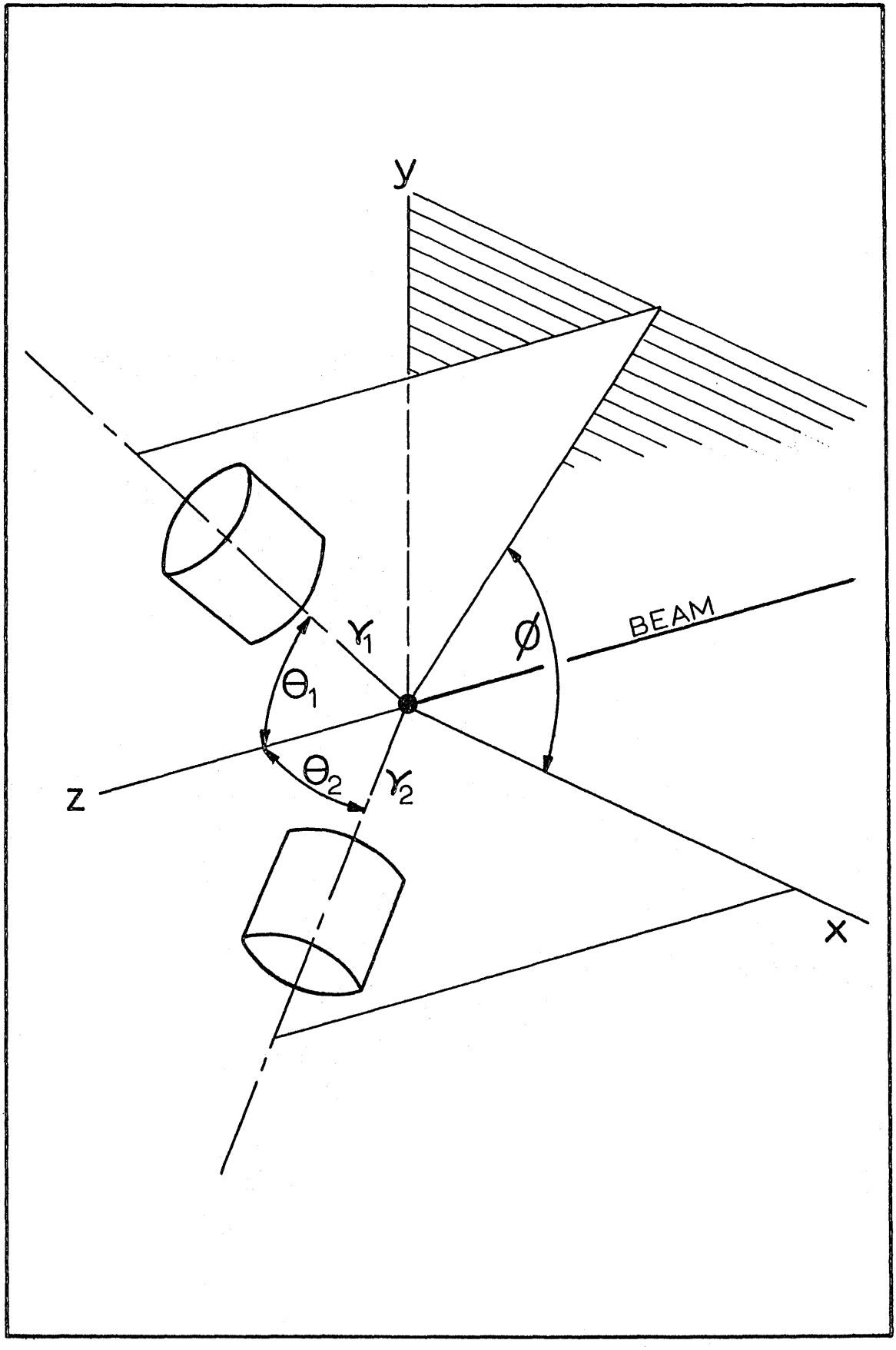

Fig. 2.2

The factors Q_K and Q_M account for the finite size of the detectors. The E^N_{KM} and h_M coefficients are the coefficients which have been tabulated. They are defined in section 2.5.

2.2.2 Multiple Cascades

If there are unobserved gamma-ray transitions between the two observed radiations as shown in Fig. 2.3, the extended formula is given by:

$$W(\Omega) = \sum_{mM} P_m(J_1)\, G_{mM}(\delta_1, \Omega)\, U_M(\delta_2) \cdots U_M(\delta_j) \cdots H_M(\delta_e). \qquad (2\text{-}5)$$

The new factors are given by:

$$U_M(\delta_a) = \frac{u_M(J_a L_a J_b) + \delta_a^2\, u_M(J_a L'_a J_b)}{1 + \delta_a^2}. \qquad (2\text{-}6)$$

The coefficients $u_M(J_a L J_b)$ are defined in section 2.5 and are tabulated along with the h_M and E^N_{KM} coefficients.

The first observed radiation does not necessarily have to be the first gamma-ray in the cascade. The angular correlation of the two observed gamma-rays from the cascade shown in Fig. 2.4 could be described as:

$$W(\Omega) = \sum_{mM} P_m(J_i)\, G_{mM}(\delta_i, \Omega)\, U_M(\delta_j) \cdots H_M(\delta_e). \qquad (2\text{-}5a)$$

If necessary, the populations of the state labeled J_i can be expressed in terms of the populations of the preceeding states according to formula (2-12) in section 2.3.

2.2.3 Angular Distributions

The angular distribution of the primary gamma-ray is obtained by averaging the triple correlation formula over all directions of the

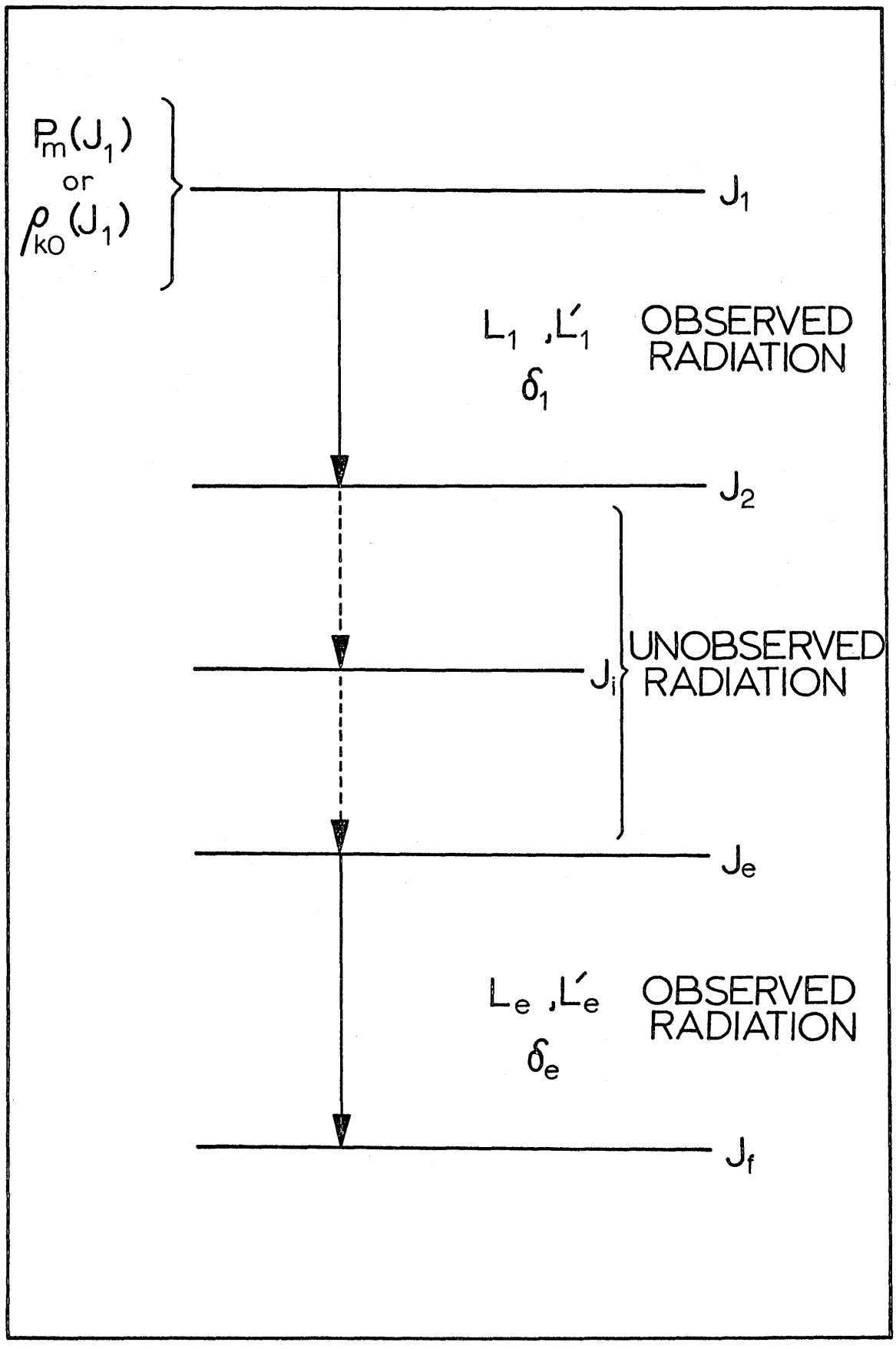
$P_m(J_1)$
or
$\rho_{kO}(J_1)$
J_1
L_1 ,L'_1
δ_1
OBSERVED
RADIATION
J_2
J_i
UNOBSERVED
RADIATION
J_e
L_e ,L'_e
δ_e
OBSERVED
RADIATION
J_f

Fig. 2.3

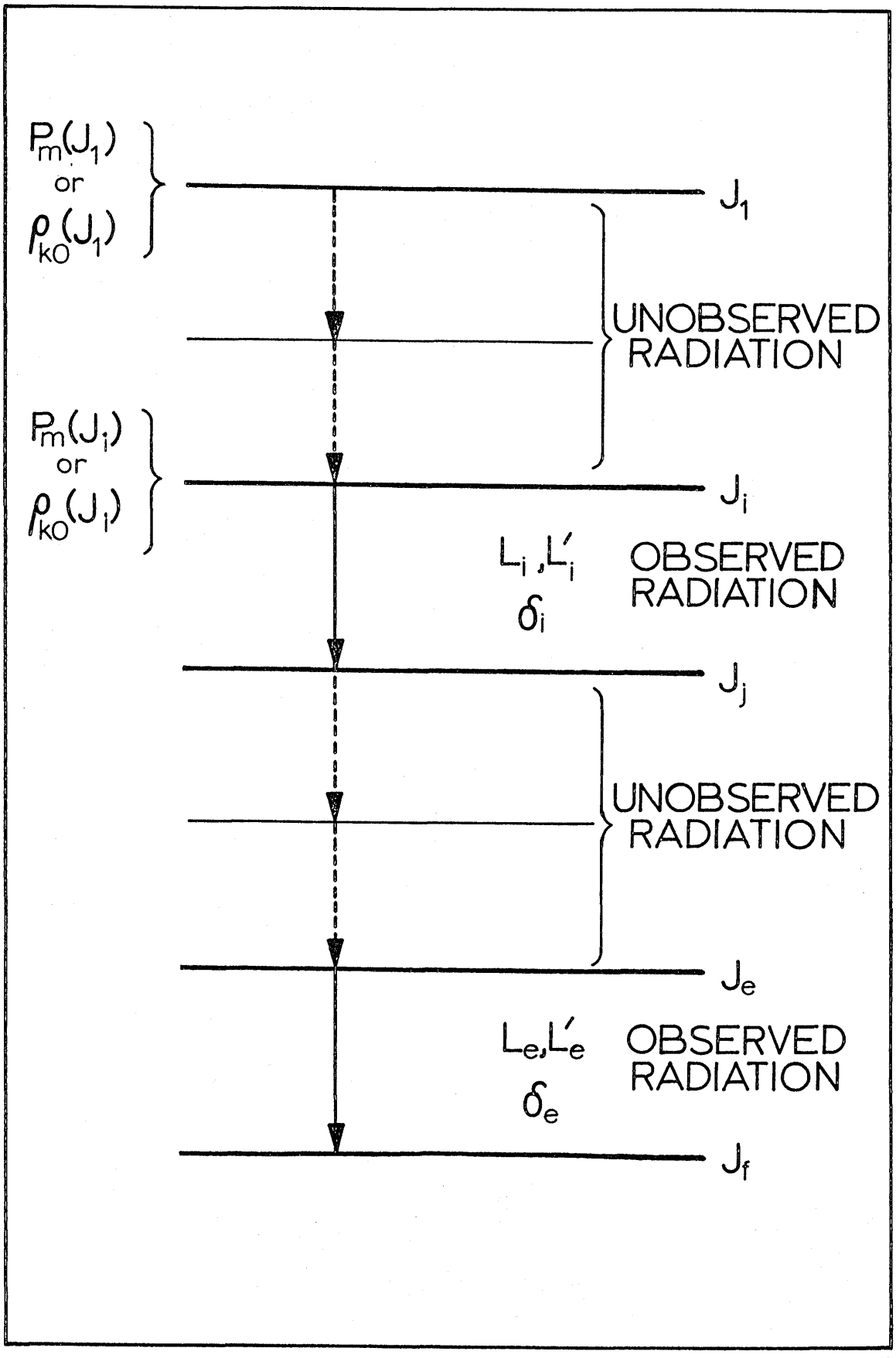
$P_m(J_1)$
or
$\rho_{kO}(J_1)$
J_1
UNOBSERVED
RADIATION
$P_m(J_i)$
or
$\rho_{kO}(J_i)$
J_i
L_i, L'_i
δ_i
OBSERVED
RADIATION
J_j
UNOBSERVED
RADIATION
J_e
L_e, L'_e
δ_e
OBSERVED
RADIATION
J_f

Fig. 2.4

secondary gamma-ray.

This provides:

$$W(\theta_1) = \sum_m P_m(J_1)\, G_{mM}(\delta_1, \theta_1)$$

$$= \sum_m P_m(J_1) \sum_{L_1 L_1'} \frac{\delta_1^{P_1}}{1+\delta_1^2} E^o_{KO}(J_1 L_1 L_1' J_2 m)\, Q_K\, X^o_{KO}(\theta_1). \qquad (2\text{-}7)$$

Similarly the angular distribution of a secondary gamma-radiation with unobserved primaries is given by the same formula (2-5) except that only the K = 0 terms remain non-zero in the expansion of the G_{mM} function. Thus:

$$W(\theta_2) = \sum_{mM} P_m(J_1)\, G_{mM}(\delta_1, \theta_2)\, U_M(\delta_2) \cdots H_M(\delta_e)$$

where

$$G_{mM}(\delta_1, \theta_2) = \sum_{L_1 L_1'} \frac{\delta_1^{P_1}}{1+\delta_1^2} E^o_{oM}(J_1 L_1 L_1' J_2 m)\, Q_M\, X^o_{oM}(\theta_2). \qquad (2\text{-}8)$$

The gamma-ray transition described by the G_{mM} function will mix incoherently as it should for an unobserved radiation because $E^o_{oM}(L\ L') = 0$ if $L \neq L'$.

These formulas for angular distributions differ from the usual Legendre polynomial expansions only by a factor $\sqrt{2K+1}$ and $\sqrt{2M+1}$ respectively.

2.3 Relations Involving Population Parameters and Statistical Tensors

The statistical tensor is related to population parameters by the transformation:

$$\rho_{ko}(J_1) = \sqrt{2J_1+1} \sum_m (-)^{J_1 - m} (J_1\, m\, J_1 - m \mid k\, 0)\, P_m(J_1). \qquad (2\text{-}9)$$

The inverse transformation is then:

$$P_m(J_1) = \frac{1}{\sqrt{2J_1+1}} \sum_k (-)^{J_1-m} (J_1\, m\, J_1, -m \mid k0)\, \rho_{k0}(J_1) \,. \tag{2-10}$$

These transformations satisfy the normalization condition

$$\rho_{00} = \sum_m P_m = 1 \,. \tag{2-11}$$

In the event that the first observed transition is preceded by one or more gamma transitions, it is useful to be able to relate the population or tensor parameters of one state to its preceding state. The relationship for populations is:

$$P_{m_2}(J_2) = 2^n \sum_{m_1} P_{m_1}(J_1)\, \frac{(L_1\, m_1+m_2\, J_2\, -m_2 \mid J_1 m_1)^2 + \delta_1^2 (L'_1\, m_1+m_2\, J_2\, -m_2 \mid J_1 m_1)^2}{1+\delta_1^2} \tag{2-12}$$

where $n = \delta_{m_1,0} - \delta_{m_2,0}$ arises from the fact that $P(m_1)$ and $P(m_2)$ are the populations of both + and - substates taken together. Due to the complicated nature of the relationship between P(m)'s it is probably desirable to express the triple correlations in terms of the populations of the state from which the first observed radiation arises. The corresponding relationship for statistical tensors is:

$$\rho_{k0}(J_2) = U_k(\delta_1)\, \rho_{k0}(J_1) \,. \tag{2-13}$$

This simple one-to-one correspondence makes it easy to write correlations in terms of the initial nuclear state even though there may be several transitions preceding the first observed transition.

2.4 Statistical Tensor Formalism

2.4.1 Ordinary Triple Correlations

The formalism for the analysis in terms of statistical tensor parameters is completely parallel to that for population parameters. The only difference is that some of the coefficients differ from each other by a linear transformation. The appropriate formulae will be stated below with the new coefficients for the sake of completeness.

The ordinary triple correlation formula for the cascade shown in Fig. 2.1 is:

$$W(\Omega) = \sum_{kM} \rho_{k0}(J_1)\, T_{kM}(\delta_1, \Omega)\, H_M(\delta_2) \qquad (2\text{-}14)$$

where

$$T_{kM}(\delta_1, \Omega) = \sum_{KN} \sum_{L,L'_1} \frac{1}{1+\delta_1^2}\, \bar{E}^N_{KN}(J_1 L_1 L'_1 J_2 k)\, Q_K\, Q_M\, X^N_{KM}(\Omega) . \qquad (2\text{-}15)$$

The coefficients $\bar{E}^N_{KM}$ are defined and tabulated along with the E^N_{KM}, h_M and u_M coefficients.

2.4.2 Multiple Cascades

The formula for multiple cascades in statistical tensor representation is:

$$W(\Omega) = \sum_{kM} \rho_{k0}(J_1)\, T_{kM}(\delta_1, \Omega)\, U_M(\delta_2) \cdots U_M(\delta_i) \cdots H_M(\delta_c) . \qquad (2\text{-}16)$$

The expression above is for a cascade of the type shown in Fig. 2.3 As with the population parameters, the statistical tensor parameters need not refer to the level from which the first gamma-ray of the cascade was emitted. The same formula would still be valid if unobserved gamma-rays preceded the first observed radiation. With statistical tensors, it is also quite simple to write the angular correlation illustrated by Fig. 2.4

in terms of the tensor parameters of the initial nuclear state.

This becomes:

$$W(\Omega) = \sum \rho_{k0}(J_1)\, U_k(\delta_1)\, U_k(\delta_2) \cdots T_{kM}(\delta_i, \Omega)\, U_M(\delta_j) \cdots H_M(\delta_e) . \qquad (2\text{-}17)$$

2.4.3 Angular Distributions

An angular distribution will result when either a transition described by the link T_{KM} or by the link H_M is unobserved. The proper formula will result in the first case by restricting M = 0 and in the second case by restricting K = 0 just as in section 2.2.3. One could just as well replace Q_M by $\delta_{M,0}$ or replace Q_K by $\delta_{K,0}$ depending on which angular distribution is desired. This result is obtained intuitively by imagining that a coincidence is still required between two detectors but with one detector subtending a solid angle of 2π.

2.5 Definitions of Coefficients

Four type of coefficients are tabulated. They can be defined as follows:

$$E^N_{KN}(J_1 L L' J_2 m) = (-)^{L'+N+1} 2^n \hat{J}_1^2 \hat{J}_2 \hat{L} \hat{L}' (L1L'-1|K0) \times \sum_k (-)^{J_1 - m} (J_1 m J_1 -m | k0)(K-NMN|k0) \begin{Bmatrix} J_2 & L & J_1 \\ J_2 & L' & J_1 \\ M & K & k \end{Bmatrix},$$

where

$$n = 2 - \delta_{L,L'} - \delta_{N,0} .$$

$$\overline{E}^N_{KM}(J_1 L L' J_2 k) = (-)^{L'+N+1} 2^n \hat{J}_1 \hat{J}_2 \hat{L} \hat{L}' (L1L'-1|K0) \times (K-NMN|k0) \begin{Bmatrix} J_2 & L & J_1 \\ J_2 & L' & J_1 \\ M & K & k \end{Bmatrix} .$$

$$h_M(J_2 L L' J_3) = (-)^{J_2 - J_3 + M - 1} 2^{1-\delta_{L,L'}} \hat{J}_2 \hat{L} \hat{L'} (L1L'-11M0) W(L J_2 L' J_2; J_3 M) .$$

$$u_M(J_a L J_b) = u_M(J_b L J_a) = (-)^{J_1 + J_2 - L} \hat{J}_a \hat{J}_b W(J_a J_a J_b J_b; M L) .$$

The symbols $\hat{J} = \sqrt{2J + 1}$. The Kronecker deltas are not to be confused with multipolarity mixing ratios. The notation for Clebsch-Gordon, Racah, and 9-J coefficients is standard.

Innumerable relationships exist between these coefficients and such coefficients as the $C^N_{KM'}$ $D^N_{KM'}$ G_γ, W, Z, F, etc. The relationships are implicit in the definitions and will be mentioned no further except to point out that in some cases, notably for u and h, the coefficients differ from other tabulated coefficients only by phase factors, "$\hat{J}$" type factors, or factors of two. In spite of their close resemblance to other coefficients, the u and h coefficients are included here for the sake of completeness and more importantly to prevent the introduction of error-conducive phase factors, etc. into the numerical calculations of correlation functions. All such factors are included in the tabulated coefficients.

Further discussion of the range, calculation, and preparation of the numerical tables is included with the actual numerical tabulations[11].

References for Section 2.

1. L.C. Biedenharn and M.E. Rose, Rev. Mod. Phys. 25, 729 (1953).

2. M.E. Rose, "Triple Correlations", ORNL-2516, Office of Technical Services. U.S. Dept. of Commerce, Washington D.C., 1958.

3. G.R. Satchler, Phys. Rev. 94, 1304 (1954).

4. S. Devons and L.J.B. Goldfarb, Encyclopedia of Physics (Julius Springer, Berlin), 42, 362 (1957).

5. A.E. Litherland and A. J. Ferguson, Can. J. Phys. 39, 788 (1961).

6. A.J. Ferguson and A.R. Rutledge, "Coefficients for Triple Angular Correlation Analysis in Nuclear Bombardment Experiments," Atomic Energy of Canada, Ltd., CRP-615, AECL-420, 1962.

7. P.B. Smith, in Nuclear Reactions, Vol II, edited by P.M. Endt and P.B. Smith, (North-Holland Publishing Company, Amsterdam, (1962))

8. P.B. Smith, Can. J. Phys. 42, 1101 (1964).

9. A. J. Ferguson, Angular Correlation Methods, to be published.

10. G.I. Harris, H.J. Hennecke, and D.D. Watson, "On the Analysis of Triple Correlation Measurements", to be published.

11. D.D. Watson, To appear in the form of an ARL Technical Documentary Report, Aerospace Research Laboratories, WPAFB, Ohio.

SECTION 3.

Analysis of Angular Correlation Data

3.1 Introduction

The analysis of data from angular correlation measurements on successive radiative transitions from aligned states is complicated by the non-linear dependence of the correlations on some of the parameters which must be determined from experimental data. It has been pointed out by Litherland and Ferguson[1] and by Smith[2] that a description of the theoretical correlations in terms of population parameters or statistical tensor parameters has the advantage of replacing the non-linear formation parameters with linear population or tensor parameters. Then for fixed values of the remaining multipolarity mixing ratios, the population or tensor parameters may be obtained by a linear least squares fit to the experimental data. HHW[3] have exploited the factorization properties of the angular correlation formalism. This factorization can be useful in applying the formalism to the analysis of data and is being used as the basis for the data analysis techniques discussed here.

A number of data analysis techniques have been described by Ferguson[4]. Specific techniques have been discussed in detail by Broude and Gove[5], Smith[2], and many others. The present work describes a system which utilizes many of the features described by the authors mentioned above. The techniques discussed here also utilize the formalism of HHW and have been used primarily on problems involving two non-linear mixing parameters.

3.2 Angular Correlation Calculations

The angular correlations between two successively emitted gamma-rays can be written as:

$$W(\Omega) = \sum_{mM} P_m G_{mM}(\delta_1, \Omega) H_M(\delta_2) , \qquad (3\text{-}1)$$

where G and H have been defined previously. The factors G and H each involve mixing parameters in the functional form $\frac{a + b\delta + c\delta^2}{1 + \delta^2}$ The magnetic substates may not all be populated due to channel spin limitations and if the final spin is zero there will be only one mixing parameter involved. On the other hand, if there should be an intermediate radiation unobserved, an additional factor $U_M(\delta_i)$ must be introduced which produces an additional mixing parameter. Data analysis problems may be classified, therefore, as in table I below:

Table I

Type	Number of mixing parameters	Number of population parameters
I	1	1
II	1	several
III	2	1
IV	2	several
V	several	1
VI	several	several

Primary emphasis will be on problems of type III and IV and some discussion of types V and VI will be given. The unique determination of parameters, of course, becomes much more difficult as their number increases.

The techniques discussed here will generally apply equally well to statistical tensors or to population parameters. The latter description is chosen partly in order that one may be able to make definite references to one system or the other. In addition, however, it is of considerable value to include in the analysis the physical constraints $P_m \geq 0$ and, in the case of channel-spin limited reactions, $P_m = 0$ for $m > m_o$. These constraints can be built into the analysis in terms of population parameters in a very simple manner. The same constraints can, of course, be written in terms of statistical tensors as,

$$\sum_k C_{mk} \rho_k \geq 0$$

and

$$\sum_k C_{mk} \rho_k = 0 \quad \text{for} \quad m > m_o ,$$

where C_{mk} are the transformation coefficients between population parameters and statistical tensors. The more complicated appearance of the constraints in the statistical tensor representation makes them more difficult, however, to include in the analysis.

3.3 General Considerations

There are at present two major classifications of techniques for solving the problem at hand: graphical techniques and "chi-squared" techniques. The graphical solutions are comprehensive, do not require large high speed computers and have been quite valuable generally. They tend to be, however, slow and cumbersome, difficult to communicate,

and relatively inaccurate in the determination of parameter values. The "chi-squared" techniques are based on the following:

$$\text{Set} \quad Q^2 = \sum_i \omega_i \left(W(i) - W^*(i)\right)^2 , \quad \text{where:} \tag{3-2}$$

ω_i is the statistical weight factor, which for the normal case of statistically uncorrelated input data is the reciprical of the variance (square of the standard deviation),

W(i) is the experimental counting rate measured at the ith set of angles θ_1^i, θ_2^i, ϕ^i, and

$W^*(i)$ is the theoretically calculated counting rate at the same angles as a function of δ_1, $\delta_2, \cdots$, P_m, $m = 1, 2, \cdots$.

The particular set of values δ_1, $\delta_2, \cdots, P_m$ is sought which minimizes Q^2. The minimum value of Q^2 will be denoted by χ^2. Use will be made of the normalized curve

$$\overline{Q}^2 = \frac{Q^2}{N}$$

with its minimum

$$\overline{\chi}^2 = \frac{\chi^2}{N}$$

where N is the number of degrees of freedom, equal to the number of experimental points minus the number of parameters adjusted in minimizing Q^2. The normalized minimum $\overline{\chi^2}$ will be near unity if the experimental data is in statistical agreement with the theoretical values for a particular set of parameters. Discussions of the statistical interpretation of $\overline{\chi^2}$ are in the literature[6].

A number of iterative techniques to find the set $\{\delta_1, \delta_2, \cdots, P_m\}$ have been explored. These techniques usually involve expanding W_i in a Taylor series around an arbitrary starting point, looking at Q^2 in that neighborhood, and then moving toward a lower point on the Q^2 surface and re-expanding until a minimum is reached. These techniques have, in practice, been frustrated by uncertain convergence due to saddle points and singularities, and the ever present possibility that a significant minimum will be missed entirely. Wherever possible, it seems advisable to parameterize the non-linear mixing ratios and use linear least squares analysis to solve for the remaining linear population parameters. Since all possible values of the mixing ratios must be investigated this process tends to require a fast computer even for two mixing ratios and computer requirements may be prohibitive for three or more. Most problems, however, involve only two non-linear parameters and even if there are three or more, the problem can be considered in "stages" as proposed in HHW and as discussed below, where each stage involves only one or two non-linear parameters.

The theoretical correlations referred to in equation (3-1) are essentially expansions of the type $\sum A^N_{KM} X^N_{KM}(\theta_1, \theta_2, \phi)$. Angular distributions are represented as $\sum A^o_{Ko} X^o_{Ko}(\theta_1)$ or $\sum A^o_{oM} X^o_{oM}(\theta_2)$ depending upon which gamma-ray of the cascade is observed. Thus, angular distributions may be treated by the computer on an equal footing with triple correlations. In practice the angular distributions are treated by the computer exactly as triple correlations except the factor $\delta_{K,o}$ or $\delta_{M,o}$ is introduced via the finite geometry correction factors. The correlations are not re-expanded in Legendre Polynomials. Also,

as indicated in equation (3-2) the Q^2 values are based on a comparison of actual experimental values at each point on a sphere with the theoretical values instead of comparing experimental expansion coefficients with theoretical expansion coefficients. Use of the experimental points is the most direct approach, provides the maximum numbers of degrees of freedom and allows the use of statistically uncorrelated input data in the analysis. It also allows full use to be made of the additional information implicit in data which is already internally normalized. In the event that triple correlation data is unnormalized between different "geometries"; or with the addition of angular distributions, which are almost certainly unnormalized with respect to the triple correlations, one must introduce normalization coefficients to be determined by least squares analysis as are the other parameters.

3.4 Normalization of Data

The technique for normalizing data arises from the following considerations: Let Ω_{ij} be the ith set of angles from the jth geometry.

Then $$Q^2 = \sum \omega_{ij} [W(\Omega_{ij}) - \eta_j W^*(\Omega_{ij})]^2$$

where η_j is the normalization constant required to consistently normalize the data of the jth geometry. One now wishes to vary η_j so as to minimize $Q^2(\eta_j)$. Since Q^2 is positive definite and quadratic in the variables η_j, the minimum in Q^2 will be the solution of the equations

$$\frac{\partial Q^2}{\partial \eta_j} = 0 \qquad \text{for } j = 1, 2, \cdots.$$

Thus one obtains:

$$\eta_j = \frac{\sum_i \omega_{ij} W(\Omega_{ij}) W^*(\Omega_{ij})}{\sum_i \omega_{ij} W^*(\Omega_{ij}) W^*(\Omega_{ij})} \quad . \tag{3-3}$$

This is equivalent to replacing $W(\Omega_{ij})$ by $N_j W(\Omega_{ij})$ and $\sigma(W(\Omega_{ij}))$ by $N_j \sigma(W(\Omega_{ij}))$ where

$$N_j = \frac{1}{\eta_j} \quad . \tag{3-4}$$

In practice it has turned out to be more convenient in the computer programs to use the factor N_j to renormalize the experimental data and the errors.

Two techniques have been used successfully for the application of equation (3-3). The first is to perform a least squares curve fit of the entire set of correlation data to a set of X^N_{KM} functions to find the best set of coefficients A^N_{KM} in the expansion

$$W(\Omega) = \sum A^N_{KM} X^N_{KM}(\Omega) \quad . \tag{3-4}$$

The least squares fitted curve is then used to derive the points $W^*(\Omega_{ij})$ referred to in equation (3-3) and the data is renormalized. The whole process is then repeated until no improvement in the χ^2 of the least squares fitted curve is obtained by further iteration. The data, thus normalized, is then fed into the program which searches for mixing parameters and population parameters for various assumed spins. This technique has proven satisfactory where enough experimental points are available, but fails when insufficient data is available to render the set of functions $X^N_{KM}(\Omega)$ linearly independent. That is, when an insufficient subspace of the $\Omega = \theta_1, \theta_2, \phi$ space is sampled in the experiment, the expansion coefficients A^N_{KM} will be indeterminate.

An alternative method which does not suffer from the above limitation is simply to find the best set $\delta_1, \delta_2, \cdots P_m$ for the unnormalized data, then normalize it using equation (3-3) and repeat the process. The iteration converges rapidly and is certain but it requires a larger number of computer operations since the problem of finding the best set of these parameters involves more computer operations than does the curve fitting used in the above mentioned process.

3.5 Single Parameter Method to Locate χ^2

A general technique for the location of the minimum in the Q^2 surface has been suggested in HHW as follows: For an assumed spin sequence,

$$W(\Omega) = \sum_{mM} P_m G_{mM}(\delta_1, \Omega) U_M(\delta_2) \cdots H_M(\delta_e) \ .$$

Set $I_{mM} = P_m U_M(\delta_2) \cdots H_M(\delta_e)$ so that

$$W(\Omega) = \sum_{mM} I_{mM} G_{mM}(\delta_1, \Omega) \ ,$$

of if ℓ stands for a unique set of mM,

$$W(\Omega) = \sum_{\ell} I_\ell G_\ell(\delta_1, \Omega) \ . \qquad (3-5)$$

Then from equation (3-3) above, $Q^2 = Q^2(I_1, I_2, \cdots I_L, \delta_1)$ and for some fixed value of δ_1, the numbers $I_1, I_2, \cdots I_L$ which minimize Q^2 can be found by ordinary linear least squares analysis. This minimum will be denoted by $\chi^2(\vec{I}, \delta_1)$ where the vector $\vec{I}$ has the components $I_1, I_2, \cdots, I_L$. A plot of χ^2 versus δ_1 can then be made after performing the calculation at several fixed values of δ_1. If no acceptable minimum is reached the

assumed spin combination can be ruled out without further analysis. If an acceptable minimum is reached at say $\delta_1 = \delta_1^o$, then the first mixing parameter is determined and one may continue by comparing the corresponding components I_ℓ^o to the set $J_\ell\, U_M(\delta_2)$ for various values of δ_2, where $J_\ell = P_m U_M(\delta_3)\cdots H_M(\delta_e)$. The analysis may then, in principle, be extended through all mixing parameters stage by stage where each "stage" has been made linear in all but one parameter. The utility and validity of the technique rests on the result obtained in the following paragraph.

In using the least squares method to choose the vector $\vec{I}$ which minimizes $Q^2(\vec{I}, \delta_1)$ it is assumed implicitly that each component I_k is free to be determined independently. This is, in fact, not the case as the set $I_1, I_2, \cdots, I_L$ may not be equal to the set $P_m U_M(\delta_1) U_M(\delta_2)\cdots H_M(\delta_f)$ for any physically possible set of values $\delta_1, \delta_2, \cdots \delta_f, P_m$, $m = 1, 2\cdots$. However since $\vec{I}$ has been chosen to precisely minimize Q^2 it must be true that

$$Q^2(\vec{I}, \delta_1) \leq Q^2(\delta_1, \delta_2, \cdots, \delta_e, P_m) \qquad (3\text{-}6)$$

for all possible values of $\delta_2, \delta_3, \cdots \delta_e, P_m$. Therefore the curve $\chi^2(\vec{I}, \delta_1)$ is in fact a lower bound to the curve $\chi^2(\delta_1, \bar{\delta}_2, \cdots \bar{\delta}_e, \bar{P}_m)$ where the bars indicate those values which minimize Q^2. Thus it is indeed true that wherever no solution exists for $\chi^2(\vec{I}, \delta_1)$, no solution will exist for any set of all other parameters $\delta_2, \delta_3, \cdots P_m$. If $\chi^2(\vec{I}, \delta_1)$ reaches an acceptable minimum for some values $\vec{I} = \vec{I}_o$, $\delta_1 = \delta_1^o$ then the analysis can proceed to the investigation for possible solutions in the variable δ_2 etc. The extension of the analysis through all of the variables is, in principle, straight forward. In some instances, however, the values I_o and δ_1^o are not well defined in the primary stage

of analysis and the continuation of the analysis to succeeding stages becomes rather difficult. If there are only two mixing ratios involved, as is frequently the case, the more straightforward technique of parameterizing both non-linear mixing ratios has been found to be free of the complications which may arise in the single parameter technique.

3.6 Double Parameterization Method

The problem of major concern here has two mixing parameters. Ideally one simply calculates the entire $\chi^2(\delta_1, \delta_2)$ surface where for each pair δ_1, δ_2, the value χ^2 is obtained by choosing the best set of linear population parameters subject to the requirement that they all be positive or zero. This solution for both mixing parameters and the associated P_m values is obtained from the minimum in the χ^2 surface. This technique is presently being used on problems involving one or two mixing parameters. The surface must be calculated at a number of separate points for fixed δ_1, δ_2. The choice of these "grid" points, the numerical output for visual display of the surface, and the constraints on P_m values are discussed individually below.

3.6.1 Grid Point Selection

In the investigation of the mixing parameter, δ, the substitution $x = \tan^{-1}\delta$ is used. Then x ranges from -90° to $+ 90^\circ$, δ ranges from $-\infty$ to $+\infty$. It has been noted[7] that this substitution renders the theoretical correlation factors sinusoidal is the variable x. This sinusoidal character is carried to the χ^2 surface and effectively renders the width of the dips in the surface independent of their position on the surface. Thus, covering the surface from -90° to $+ 90^\circ$ with a square

grid of say 5^{o} intervals in the angular variables covers the entire range of mixing parameters from $-\infty$ to $+\infty$ and does so with the same degree of detail over the entire surface. In practice, grids of as fine as 2^{o} have been used. The 2^{o} grid results in just over 8000 grid points and is more than sufficient to define all dips in the surface. A program has been written for the IBM 7094 computer which can cover an 8000 point grid in less than one minute including the computation of the necessary E and H coefficients and X^{M}_{KM} functions. The computation of E and H coefficients is included in the program so that the only input to the computer will be the experimental data and spin combinations.

3.6.2 Display of the χ^2 surface

Rather than write out the χ^2 value at every grid point the computer provides two curves which carry the significant information. For an NxN grid the first curve is $\chi^2(\overline{P}_m, \delta_1^i, \overline{\delta}_2)$ for $i = 1, 2, \cdots, N$ where $\overline{P}_m$ and $\overline{\delta}_2$ indicate the choice among all possible values which renders χ^2 a minimum. The second curve is $\chi^2(\overline{P}_m, \overline{\delta}_1, \delta_2^i)$ for $i = 1, 2, \cdots, N$. These curves are simply the projections or "shadows" of the χ^2 surface on the δ_1 and δ_2 planes. This technique removes any chance of missing a minimum and it provides a reasonable visual image of the entire surface as well as the minimum values of δ_1 and δ_2 while maintaining a tractable output. In addition, it will be pointed out in section 3.8 that the projection technique accounts for correlation errors among the various parameters whereas a slice of the surface would not.

3.6.3 Constraints on Population Parameters

In practice, it has been found that the inclusion of the physical constraints $P_m \geq 0$ into the calculation of the χ^2 surface is highly

desirable. The χ^2 surface will then result from the choice of non-negative population parameters which render $\chi^2(\delta_1, \delta_2, P_m)$ a minimum at each grid point (δ_1, δ_2). In order to find the proper set of P_m values, the calculation of χ^2 is first carried out with no restrictions on P_m. If one or more values of P_m turn out to be negative, these values are set equal to zero and the calculation is repeated using only the remaining non-zero P_m values. The elements of the normal matrix which are required for the latter calculation are already in the computer memory from the first calculation and the increase in computer time is slight. This procedure actually provides the lowest χ^2 value within the limitation $P_m \geq 0$ due to the fact that the Q^2 surface is precisely quadratic in the P_m variables and thus increases monotonically with P_m as P_m increases from the original minimum point.

3.7 Simultaneous Analysis of Data from Separate Experiments

A final question to be considered is that of mixing the results of data obtained from two different cascades or from two or more resonances which involve a common spin or mixing parameters, in order to obtain a single resultant χ^2 curve. The question is first considered for problems with only one population parameter (Type III) and is illustrated by example.

Suppose the situation shown in Fig. 3.1 exists, where the level J_2 is populated by gamma-ray transitions from three different resonance levels of the same nucleus. It is presumed that for a given choice of J_2 and J_3 one already has found J_{R_i}, δ_{R_i}, J_{R_2}, δ_{R_2}, J_{R_3}, δ_{R_3} which minimize the χ^2 values for each of the three cascades separately. Then by the definition of the "shadow plots" the properly mixed plot for the common

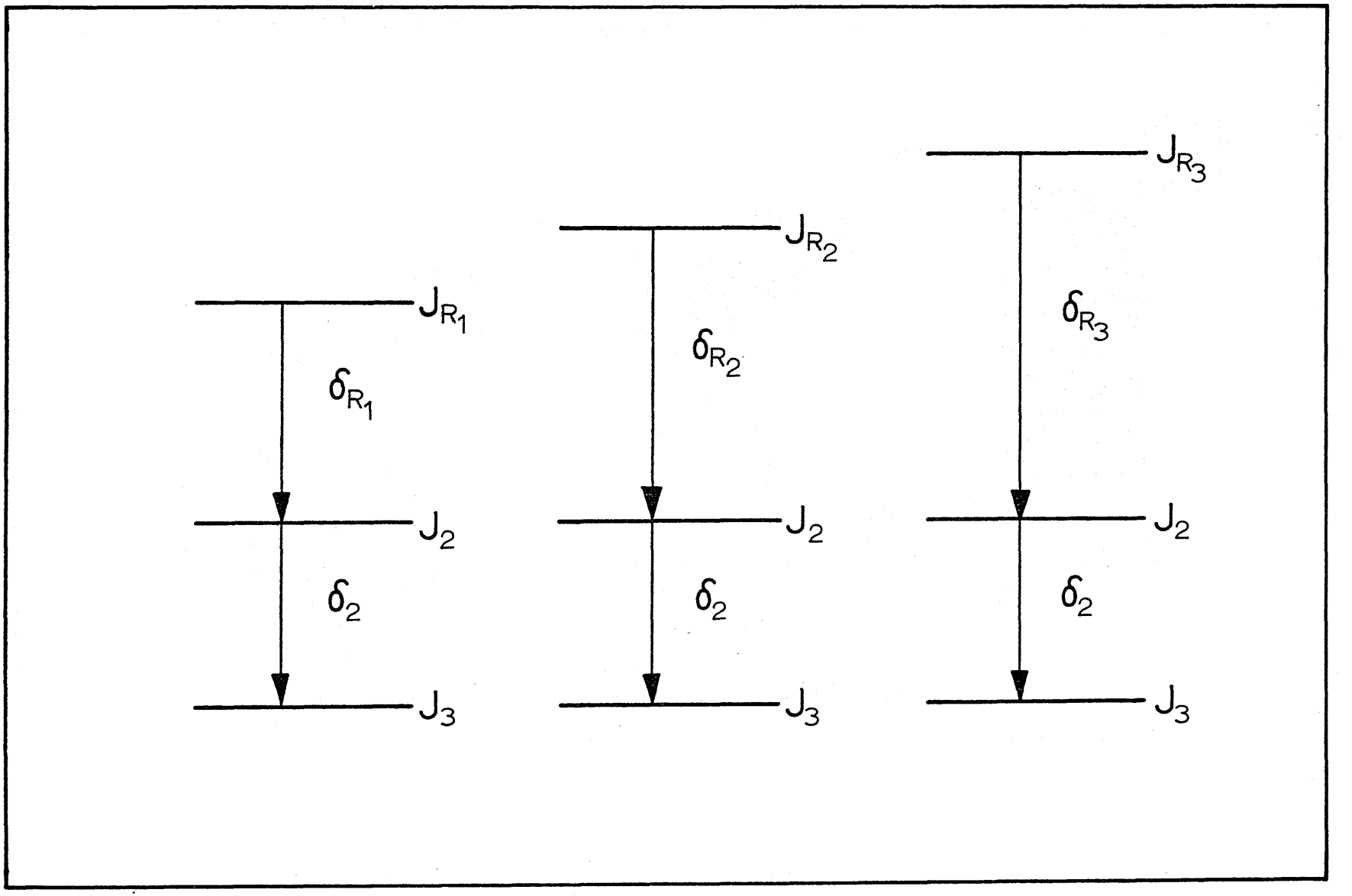
J_{R_1}
δ_{R_1}
J_2
δ_2
J_3
J_{R_2}
δ_{R_2}
J_2
δ_2
J_3
J_{R_3}
δ_{R_3}
J_2
δ_2
J_3

Fig. 3.1

variable δ_2 is:

$$\bar{\chi}^2_{Tot.}(\delta_2^i) = \frac{N_1 \bar{\chi}^2_1(\delta_2^i) + N_2 \bar{\chi}^2_2(\delta_2^i) + N_3 \bar{\chi}^2_3(\delta_2^i)}{N_1 + N_2 + N_3} , \qquad (3\text{-}7)$$

where N_1, N_2, and N_3 are the number of degrees of freedom of the individual experiments and as before the bars over χ^2 indicate that they are the normalized curves which are produced by the computer in the analysis of the separate experiments. A similar expression is obtained for the common spin J_2:

$$\bar{\chi}^2_{Tot.}(J_2) = \frac{N_1 \bar{\chi}^2_1(J_2) + N_2 \bar{\chi}^2_2(J_2) + N_3 \bar{\chi}^2_3(J_2)}{N_1 + N_2 + N_3} \qquad (3\text{-}8)$$

where $\bar{\chi}^2_1(J_2)$ is the lowest value of $\bar{\chi}^2_1$ obtainable for a particular choice of J_2, and so on for $\bar{\chi}^2_2$ and $\bar{\chi}^2_3$. The process is extended in the same manner to cover other overlapping situations such as for the spin J_1 or the mixing parameter δ_1 as obtained from the various possible angular distributions and triple correlations which can be performed with the gamma rays indicated by Fig. 3.2. Since these mixed curves are all obtained simply by the weighted addition of separate "shadow" curves obtained in the individual analyses, the actual mixing of information is rather trivial.

If more than one magnetic substate is populated, then the mixing of overlapping P_m values can be, in principle, accomplished in the same way but becomes much more complicated in practice since the P_m values are not parameterized as are the spins and mixing parameters. The mixing of magnetic substate values requires major complications in computation and is not considered practical at present.

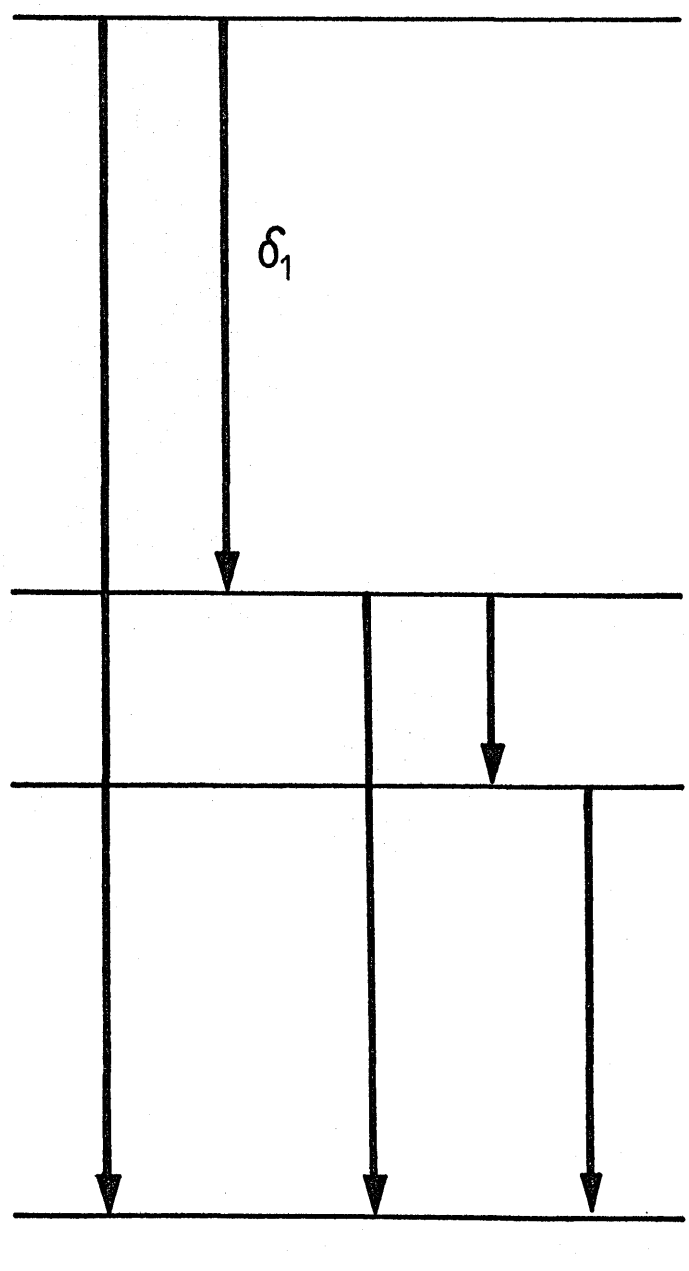

Fig. 3.2

3.8 Analysis of Errors

A few remarks are included here to indicate the method of error determination in the measured parameters. The determination must include the errors in the parameterized mixing ratios including the effects of correlation errors. First, a general analytic approach is outlined. It is shown in the next section that much of the error information is already contained in the "shadow" plots and, in fact, they will suffice to determine the errors in the mixing ratios with no additional analysis. Although it is much less convenient, one could even deduce the correct correlated errors of the population parameters from their values and uncorrelated errors over the region of the "error ellipse".

3.8.1 Analytic Error Determination

The essential basis for the analytic determination of errors in the parameters is the linearization of the theoretical angular correlation functions, or equivalently, the quadratic approximation of the Q^2 surface in the region of the minimum.

Suppose the search program has found values δ_1^o , $\delta_2^o, \cdots, \delta_e^o, P_m^o$, $m = 1, 2, \cdots$ at the grid point nearest to the minimum in the Q^2 surface.

Set

$$\begin{aligned} \epsilon_1 &= \delta_1 - \delta_1^o \\ \epsilon_2 &= \delta_2 - \delta_2^o \\ &\vdots \\ \epsilon_e &= \delta_e - \delta_e^o \\ \epsilon_{e+1} &= P_1 - P_1^o \\ &\vdots \end{aligned} \qquad (3\text{-}9)$$

Then $$W^*(i) \approx W_o^*(i) + \sum_k \epsilon_k \frac{\partial W_o^*(i)}{\partial \epsilon_k}$$ so that

$$Q^2 = \sum_i \omega_i \left(W(i) - W_o^*(i) - \sum_k \epsilon_k \frac{\partial W_o^*(i)}{\partial \epsilon_k} \right)^2 . \qquad (3\text{-}10)$$

The subscript 0 indicates that the quantity is to be evaluated at $\delta_1^o, \delta_2^o, \cdots, P_m^o$. The corresponding normal matrix is

$$C_{\ell\ell'} = \sum_i \omega_i \frac{\partial W^*(i)}{\partial \epsilon_\ell} \frac{\partial W^*(i)}{\partial \epsilon_{\ell'}} = \frac{1}{2} \frac{\partial^2 Q^2}{\partial \epsilon_\ell \, \partial \epsilon_{\ell'}} \qquad (3\text{-}11)$$

and the variance-covariance or error matrix for the correction factors is the inverse of C, i.e.,

$$E = C^{-1} . \qquad (3\text{-}12)$$

But these are just the desired errors since the position of the minimum is now given by

$$\delta = (\delta^o + \epsilon) \pm \sigma(\epsilon) .$$

Thus:

$$\begin{aligned} \sigma^2(\delta_i) &= \sigma^2(\epsilon_i) = E_{ii} \qquad && i = 1, 2, \cdots, e \\ \sigma^2(P_i) &= \sigma^2(\epsilon_i) = E_{ii} \qquad && i = e+1, e+2, \cdots . \end{aligned} \qquad (3\text{-}13)$$

Also, the correction factors are obtained from

$$\epsilon_i = \sum_j E_{ij} Y_j , \qquad (3\text{-}14)$$

where $$Y_j = \sum_i \omega_i \left(W(i) - W_o^*(i) \right) \frac{\partial W_o^*(i)}{\partial \epsilon_j} ,$$

as a result of linear least squares analysis.

The matrix elements $C_{\ell\ell'}$ can be calculated in several ways. Either of the derivatives $\frac{\partial W_o^*}{\partial \epsilon_\ell}$ or $\frac{\partial^2 Q^2}{\partial \epsilon_\ell \partial \epsilon_{\ell'}}$ of equation (3-11) may be calculated analytically since the functional form of W^* (and, hence, also of Q^2) is known. Alternatively the numerical second derivatives of Q^2 may be readily calculated using quantities which are available in the computer.

In the case where several population parameters are involved, the errors in the normalized quantities

$$R_m = \frac{P_m}{\sum_k P_k}$$ are desired. If E_{ij} is the error matrix corresponding to the population parameters and $S = \sum_K P_K$, then the variance in the ratio can be expressed as:

$$\sigma^2(R_m) = R_m^2 \left[\frac{E_{mm}}{P_m^2} + \frac{\sum_{ij} E_{ij}}{S^2} - 2 \frac{\sum_i E_{im}}{P_m S} \right] , \qquad (3\text{-}15)$$

This expression is derived from the error techniques discussed in Appendix I of this thesis.

It should be kept in mind that the analytic technique will fail if the Q^2 surface becomes non-quadratic near its minimum and also that it provides only the internal or purely statistical errors in the measurement. Thus, care must be exercised in interpreting results where doubt exists about the relative importance of systematic errors and non-quadratic behavior.

3.8.2 Graphical Error Determination

Assume that the Q^2 surface depends on two independent variables and is quadratic in the region of the minimum so that,

$$Q^2 = Q_0^2 + Ax^2 + By^2 + Cxy \quad , \qquad (3\text{-}16)$$

where Q_o^2 is the value at the minimum and x and y are the coordinates of displacement from the minimum. A contour in the Q^2 surface at the value $Q^2 = Q_o^2 + 1$ would have the form of an ellipse. By a transformation to new coordinates whose axes coincide with the major and minor axes of the ellipse we have

$$Q^2 = \alpha x'^2 + \beta y'^2 + Q_o^2 \quad . \tag{3-17}$$

From equation (3-11) the normal matrix corresponding to this form is:

$$C = \begin{pmatrix} \alpha & 0 \\ 0 & \beta \end{pmatrix} , \tag{3-18}$$

and the error matrix which will specify the errors in the x' and y' coordinates is therefore

$$E' = \begin{pmatrix} 1/\alpha & 0 \\ 0 & 1/\beta \end{pmatrix} . \tag{3-19}$$

Again consider the contour $Q^2 = Q_o^2 + 1$. In the new coordinate system this contour has the form

$$\alpha x'^2 + \beta y'^2 = 1 \quad . \tag{3-20}$$

Comparing equations (3-20) and (3-19), one may observe that the squares of the semi-major and semi-minor axes of the ellipse are the variances, and thus the semi-major and semi-minor axes of this "error" ellipse are the values of one standard deviation. This discussion is illustrated in Fig. 3.3. The error matrix can now be transformed back into the x-y coordinates and becomes:

$$E = \begin{pmatrix} \sigma^2(x')\cos^2\theta + \sigma^2(y')\sin^2\theta & \sin\theta\cos\theta\,(\sigma^2(x') - \sigma^2(y')) \\ \sin\theta\cos\theta\,(\sigma^2(x') - \sigma^2(y')) & \sigma^2(x')\sin^2\theta + \sigma^2(y')\cos^2\theta \end{pmatrix} \tag{3-21}$$

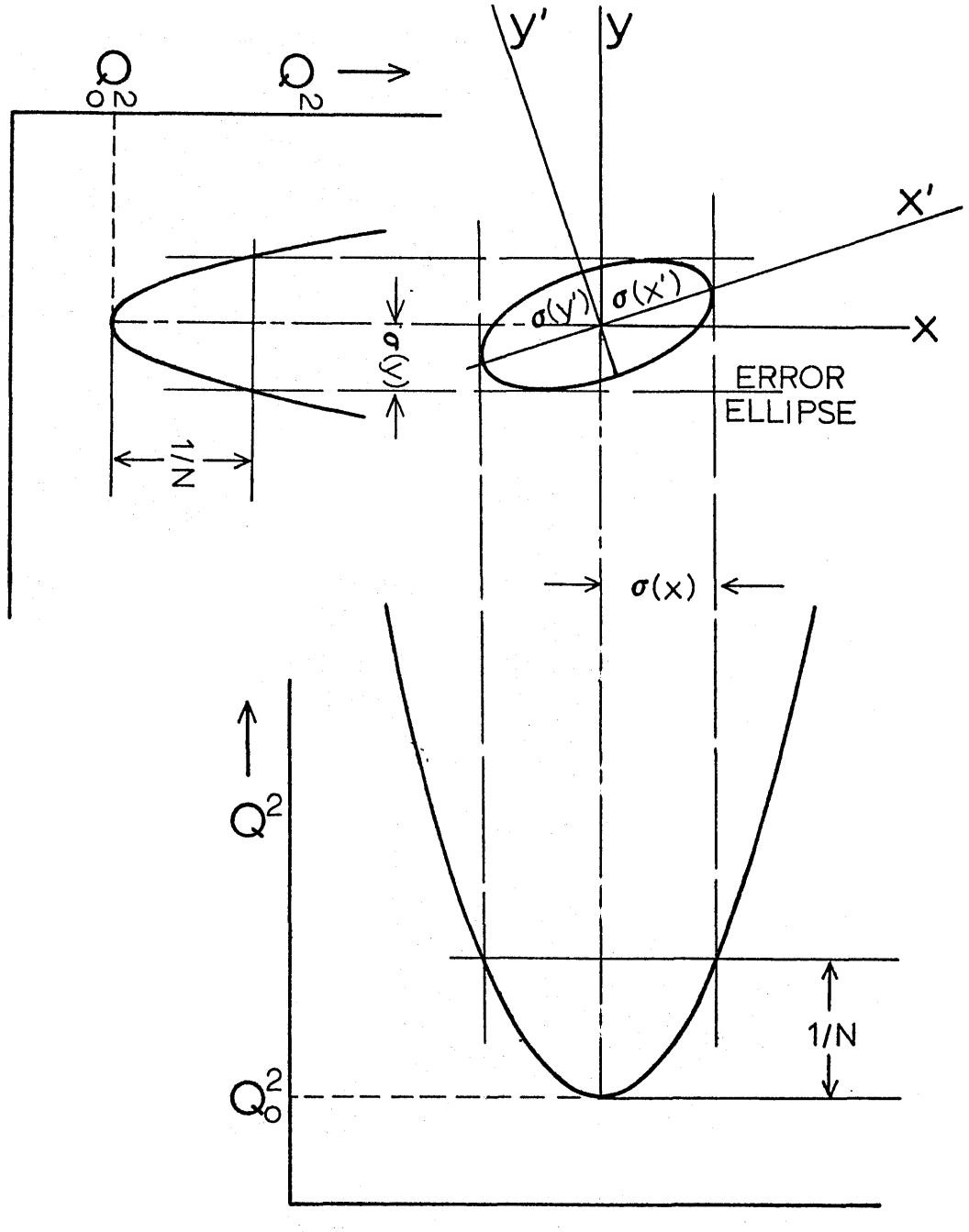
y'
y
Q_{o2}
Q_2
x'
x
$\sigma(y')$
$\sigma(x')$
$\sigma(y)$
ERROR
ELLIPSE
1/N
$\sigma(x)$
Q^2
Q_o^2
1/N

Fig. 3.3

where θ is the angle of rotation of the ellipse. Geometrical considerations reveal that the diagonal terms of the error matrix are just the squares of the projections of the outermost points of the ellipse onto the x and y axes as shown in Fig. 3.3. This is exactly the result one would obtain by cutting off the "nose" of the shadow curves at $Q^2 = Q_o^2 + 1$; or $\overline{Q}^2 = \overline{Q}_o^2 + 1/N$ if the curves are normalized.

Thus a remarkably simple prescription emerges: The half width of the shadow plot at $\overline{Q}^2 = \overline{Q}_o^2 + 1/N$ is one standard deviation in the variable for which it is plotted and account is properly taken of the correlation error with the other variable. This result is most useful when the only variables involved are two mixing ratios but can be applied as well to problems involving population parameters.

3.9 Discussion

It has been the purpose of this discussion to enumerate in a general way the principle techniques which are being currently employed in the analysis of angular correlation data. The techniques are hopefully oriented towards the evolution of a computer program which requires as input only the "raw" experimental data and which provides at the output a complete analysis of the data. At least for some cases of interest it now appears possible to come surprisingly close to this goal. The computer program which has been used for the analysis of the data from the $S^{34}(p,\gamma)Cl^{35}$ reaction is discussed in Appendix II. A somewhat more generalized version of this program is also being used presently to analyze data from reactions with channel spin greater than one-half. The angular correlation problems which have so far been encountered have been adequately solved by the methods discussed above.

References for Section 3.

1. A.E. Litherland and A.J. Ferguson, Can. J. Phys. 39, 788 (1961).

2. P.B. Smith, Can. J. Phys. 42, 1101 (1964).

3. G.I. Harris, H.J. Hennecke, and D.D. Watson, "On the Analysis of Triple Correlation Measurements", to be published.

4. A.J. Ferguson, Angular Correlation Methods, to be published.

5. C. Broude and H.E. Gove, Annals of Physics, 23, 71 (1963).

6. Wapstra, Nijgh and Van Lieshout, Nuclear Spectroscopy Tables, North Holland Publishing Co., Amsterdam (1959).

7. D.D. Watson, R.A. Moore, G.I. Harris and L.W. Seagondollar, Nuclear Instruments and Methods, 23, 157 (1963).

SECTION 4

Introduction to the Experimental Work on $S^{34}(p,\gamma)Cl^{35}$

4.1 Review of Cl^{35} Properties and Comparison with Models

In shell model nomenclature, Cl^{35} would have a single $1d_{3/2}$ proton and a pair of $1d_{3/2}$ neutrons beyond the filled $2s_{1/2}$ subshell. The experimental energy level structure of the low lying levels is shown in Fig. 4.1 along with some theoretical calculations as follows:

1. jj-coupling shell model by Pandya[1].
2. jj-coupling shell model by Arima[2].
3. Nillson model by Bhatt[3].
4. Asymmetric Core Rotator model by Chi and Davidson[4].
5. Shell model calculations by Glaudemans[5].

The first three level schemes are based upon configurations of the $d_{3/2}$ nucleons. Bhatt[3] has pointed out that in the region of deformations relevant to Cl^{35} ($\eta \approx -2$), the last filled Nilsson orbit (No. 9) crosses the first unfilled orbit (No. 8). This results in the likelihood of low energy core excitations in which one of the $2s_{1/2}$ nucleons is elevated into the $1d_{3/2}$ subshell. In such cases an extreme single particle model would fail. This could explain the poor agreement and particularly the failure of these single particle models to predict the spin 1/2 first excited state in Cl^{35}. The recent model by Glaudemans[5] allows for configuration mixing of all particles outside an inert Si^{28} core. It is particularly noteworthy that the first excited state of the Glaudeman calculations turns out to be predominately an $(S_{1/2}^{3})_{1/2}\ (d_{3/2}^{4})_{0}$

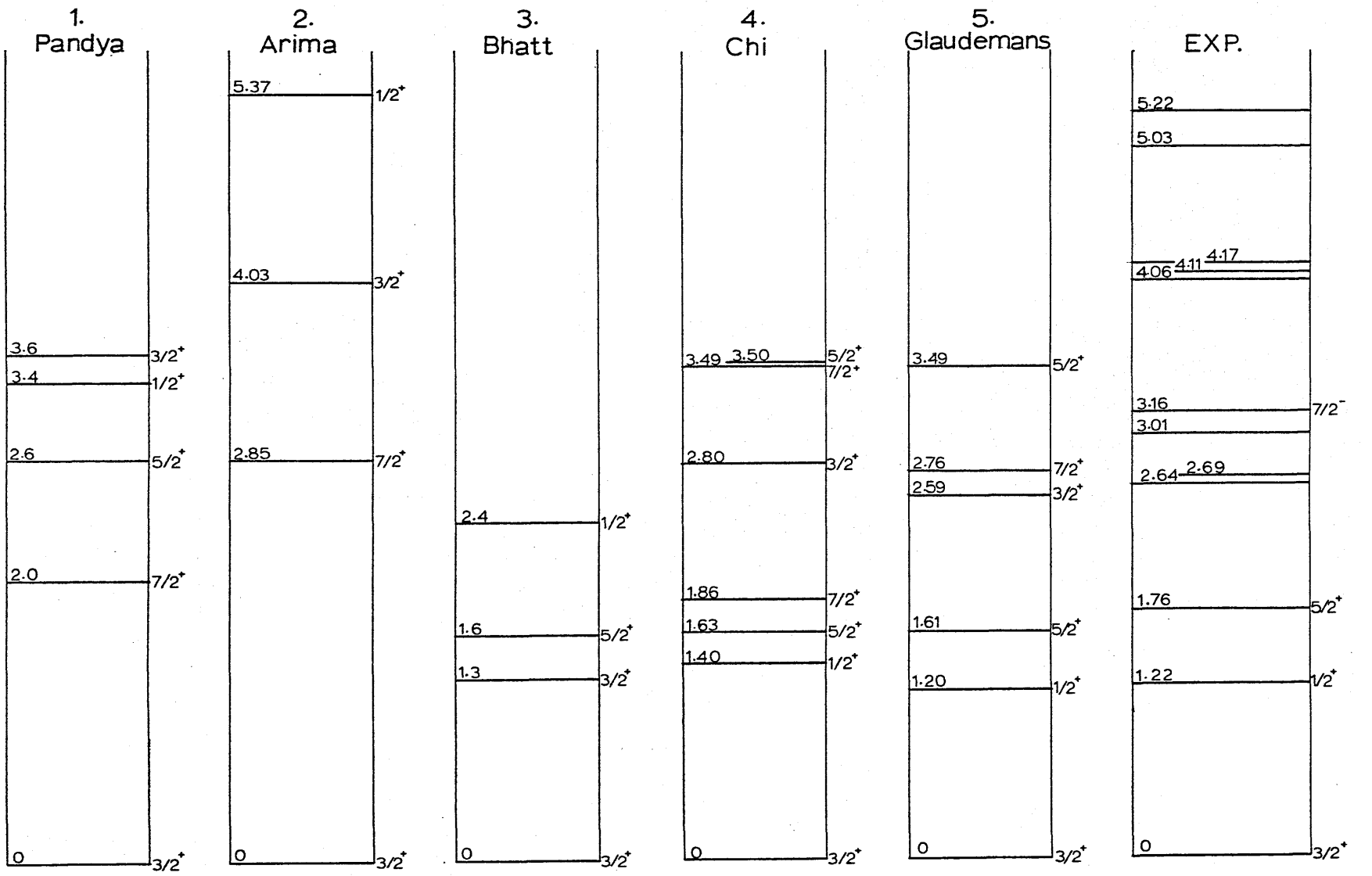
1.
Pandya
3.6
3/2+
3.4
1/2+
2.6
5/2+
2.0
7/2+
0
3/2+
2.
Arima
5.37
1/2+
4.03
3/2+
2.85
7/2+
0
3/2+
3.
Bhatt
2.4
1/2+
1.6
5/2+
1.3
3/2+
0
3/2+
4.
Chi
3.49
3.50
5/2+
7/2+
2.80
3/2+
1.86
7/2+
1.63
5/2+
1.40
1/2+
0
3/2+
5.
Glaudemans
3.49
5/2+
2.76
7/2+
2.59
3/2+
1.61
5/2+
1.20
1/2+
0
3/2+
EXP.
5.22
5.03
4.17
4.11
4.06
3.16
7/2-
3.01
2.69
2.64
1.76
5/2+
1.22
1/2+
0
3/2+

Fig. 4.1

configuration rather than $(S_{1/2}^{4})_0 (d_{3/2}^{3})_{1/2}$. This supports the observations of Bhatt. Glaudeman's calculations also indicate that the 3/2+ ground state of Cl^{35} is a reasonably pure single particle configuration and that the 5/2+ second excited state is a highly mixed configuration, again involving components in the S^3d^4 configuration.

The absence of a sufficient number of experimentally known properties of Cl^{35} is clearly a hinderance to the development of successful models with which to describe its structure. The remainder of this thesis concerns the experimental determination of some spins, parities, and gamma-ray mixing and branching ratios for the Cl^{35} nucleus by a study of gamma-rays from the $S^{34}(p,\gamma)Cl^{35}$ reaction.

Much of the past work on Cl^{35} has been summarized by Endt and Van der Leun[6]. The excitation energies of several low lying levels have been measured by Endt et. al.[7] Approximately 70 $S^{34}(p,\gamma)Cl^{35}$ resonances in the proton energy range from .6 to 1.2 MeV have been identified by Hyder[8]. Decay schemes and branching ratios for several resonances between proton energies from 0.76 to 1.2 MeV have been obtained by Hazewindus et. al.[9]. Yang Tan[10] has investigated the decay schemes of several other resonances. Some of these resonances have been chosen for angular distribution, triple correlation, and polarization measurements. Two such resonances will be discussed in Section 5. A brief review of target making techniques and experimental procedures will be presented below.

4.2 Target Preparation

Targets were made from elemental sulfur enriched to 37% in S^{34}.

Sulfur, in elemental form, is not a suitable target material since thin films of sulfur evaporate quite rapidly under high vacuum. Targets of CdS were prepared by evaporating a thin layer of cadmium metal on top of sulfur immediately after the sulfur had been evaporated upon outgassed .005" thick tantalum disks. The disks, so prepared, were then heated under vacuum to a nearly red heat until a color change occurred over the entire face of the target. The color change was taken to indicate the formation of CdS. These targets proved to be stable and could withstand relatively high temperatures in vacuum. The target disks were then attached to a 1/16" aluminum backing by a thin layer of low vapor pressure, high temperature epoxy resin. The epoxy cement apparently held the aluminum in good enough thermal contact with tantalum target backing to act as an effective heat sink. With this arrangement, a target dissipation of 20 watts could be maintained without target deterioration.

4.3 Experimental Methods

The $S^{34}(p,\gamma)Cl^{3}$% reaction was initiated by the proton beam from the University of Kansas 3 MeV electrostatic accelerator (H.V.E.C. model KN3000). Energy defining slits placed at the focal point of a 25^{o} analyzing magnet provided energy resolution of about 1 keV for a 1.5 MeV beam. Energy measurements were made with a N.M.R. fluxmeter in the analyzing magnet. Energy calibration was referenced to the $Al^{27}(p,\gamma)Si^{28}$ resonance at 992 keV and the $L_i^{7}(p,n)$ threshold at 1881 keV. For the latter reaction, neutrons were detected at 0^{o} to the beam axis by a LiI crystal with a plastic moderator. After an

initial energy measurement of the prominent S^{34} resonance at 1214 $\pm$ 1 keV, this resonance was used to check the energy calibration at frequent intervals. A three element electric quadrupole lens focussed the proton beam through a defining aperature and an anti-scatter aperature before the beam struck the target. The target end of the beam tube was evacuated by a cold-trapped, silicon-oil diffusion pump. Another liquid nitrogen cold trap was in line with the beam tube prior to the target chamber.

Most of the work was performed with two 5" x 5" NaI(Tl) crystals, having 9% to 9.5% resolution on the 661 keV line from Cs^{137}, and with one 9" diameter by 4" thick NaI(Tl) cyrstal having 8.5% to 9% resolution. Line shape calibrations of the crystals were obtained by observing monoergic gamma-rays from several well known reactions[10].

Gamma-induced pulses from the scintillation counters entered charge sensitive preamplifiers. Output pulses from the preamplifiers passed through terminated coaxial cables to the inputs of double delay line amplifiers. Pulse height stabilization was maintained by commercial gain-drift compensators which were set to observe the 661-keV line from a radioactive Cs^{137} source kept near the crystals. A 400 channel pulse height analyzer was available which could be split into two groups of 200 channels or four groups of 100 channels with separate input circuits. In many cases 100 channel resolution will suffice for the coincident spectra of triple correlation measurements. In such cases one can record 4 independent triple correlation geometries simultaneously. Figs. 4.2 and 4.3 show the general features of two electronic arrangements which were used for this purpose. With the arrangement shown

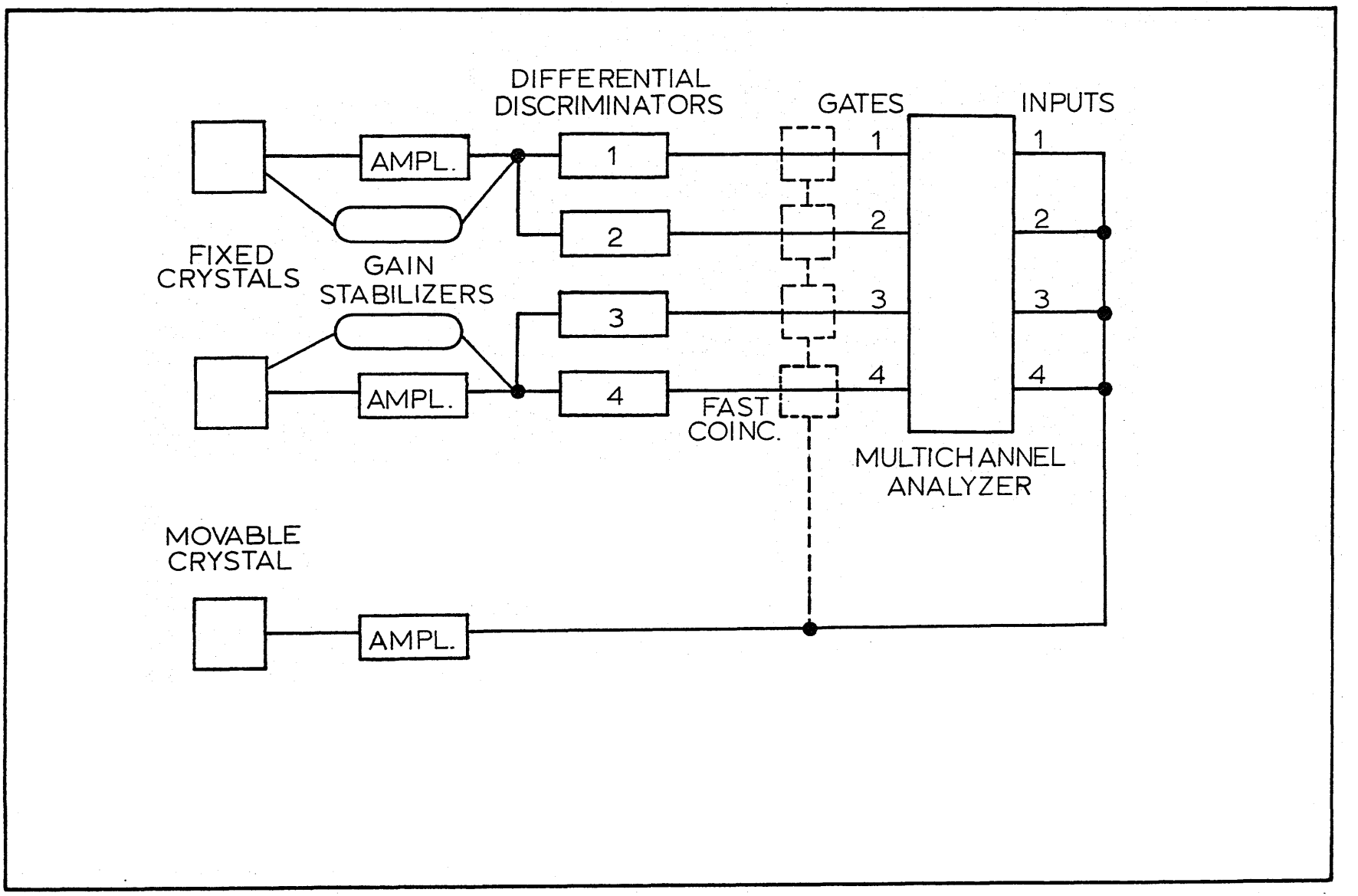
DIFFERENTIAL
DISCRIMINATORS
GATES
INPUTS
AMPL.
1
2
3
4
FIXED
CRYSTALS
GAIN
STABILIZERS
AMPL.
FAST
COINC.
MULTICHANNEL
ANALYZER
MOVABLE
CRYSTAL
AMPL.

Fig. 4.2

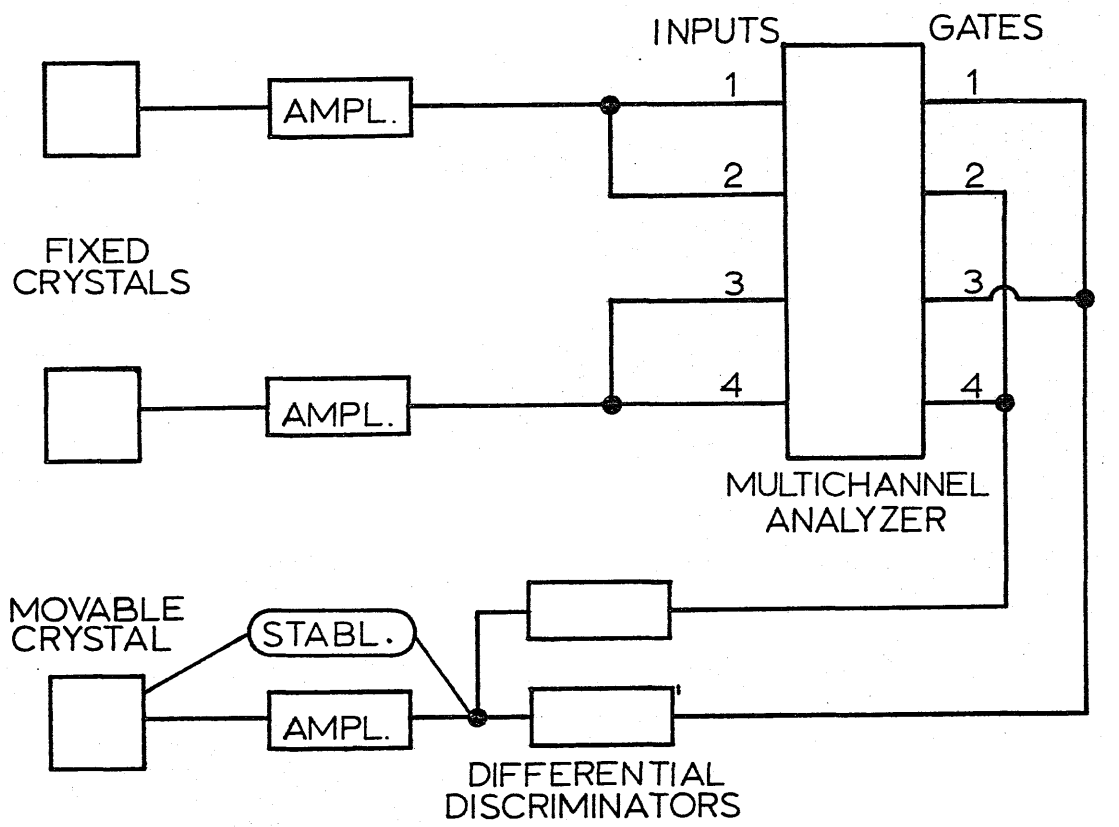
INPUTS
GATES
AMPL.
1
1
2
2
FIXED
CRYSTALS
3
3
AMPL.
4
4
MULTICHANNEL
ANALYZER
MOVABLE
CRYSTAL
STABL.
AMPL.
DIFFERENTIAL
DISCRIMINATORS

Fig. 4.3

in Fig. 4.3 extreme caution must be exercised to prevent position dependent gain shifts in the movable crystal. In the other arrangement, gain shifts in the movable counter are recorded and compensation is possible. The circuits shown will have a coincidence resolution time of about 3 microseconds as determined by the multichannel pulse height analyzer. Although this is adequate for many (p,γ) reactions, in some cases an additional fast time coincidence requirement was imposed on crossover pickoff pulses derived from the outputs of the double delay line amplifiers. In this case the gate pulse was provided to the multichannel analyzer only if prompt time coincidence between the crystal pairs was established. The position of the fast time coincidence units is indicated by the dashed lines in Fig. 4.2. This allowed time resolution as fast as 10 ns. but the coincidence units were operated usually with a resolution of about 50 ns. in order to avoid the possible loss of true coincident events due to either random or pulse height dependent time jitter of the crossover pulses.

Anisotropies in the goniometer and target chamber were checked by the observation of the isotropic gamma-ray from the de-excitation of the spin 1/2 level in P^{31} resulting from the capture of 620 keV protons by Si^{30}. Accurate correlation measurements also depend on the proper normalization of individual measurements at each angular setting. This normalization was accomplished by monitoring a prominent gamma-ray of the reaction (such as from a ground state transition) in one or more fixed crystals. This method is satisfactory so long as any unavoidable background radiation is negligible in comparison with the reaction gamma-ray which is chosen for normalization purposes.

Otherwise, it may be necessary to monitor the coincidence counting rate between two reaction gamma-rays in cascade in order to properly determine the reaction yield.

References for Section 4

1. S. P. Pandya, Prog. Theor. Phys. 19, 404 (1958)
2. A. Arima, Prog. Theor. Phys. 19, 421 (1958)
3. K. H. Bhatt, Nuclear Phys. 39, 375 (1962)
4. B. E. Chi and J. P. Davidson, Phys. Rev. 131, 366 (1963)
5. P. W. M. Glaudemans, G. Weichers and P. J. Brussard, Nuclear Phys. 56, 548 (1964)
6. P. M. Endt and C. Van der Leun, Nuclear Phys. 34, 1 (1962)
7. P. M. Endt, C. H. Paris, A. Sperduto and W. W. Buechner, Phys. Rev. 103, 961 (1956)
8. A. K. Hyder, Thesis, Air Force Institute of Technology, USAF, (1964)
9. N. Hazewindus, W. Lourens, A. Scheepmaker and A. H. Wapstra, Physica 29, 681 (1963)
10. Yang Tan, Thesis, University of Kansas, (1964)

SECTION 5

The Resonances at 1214 keV and 1905 keV in the $S^{34}(p,\gamma)Cl^{35}$ Reaction

5.1 Introduction

The resonance in the $S^{34}(p,\gamma)Cl^{35}$ reaction at Ep = 1214 keV has provided considerable information concerning the properties of Cl^{35}. Work on this resonance has also been of value in the development of techniques of measurement and data analysis. The data is ideally suited as a test for the data reduction and analysis procedures developed thus far. Another resonance at Ep = 1905 keV decays through the same level at 3.16 MeV as does the 1214 keV resonance and the studies of both resonances are so closely related that they will be discussed together. The various measurements are discussed in the order they were performed in order to preserve the logic in the sequence of the measurements.

The 1214 keV resonance has been observed by a number of investigators[1, 2, 3]. It is the strongest resonance in the $S^{34}(p,\gamma)Cl^{35}$ reaction in the proton energy range below 2 MeV. The resonance strength of the resonance is reported by Hazewindus[1] as $\omega\gamma$ = 2 ev. The decay scheme is rather curious in that the resonance level decays almost entirely (> 95%) to only the one level at 3.16 MeV excitation. The spins of both the resonance level and the 3.16-MeV level have been reported by Antuvjev et.al.[2] to be 7/2. The spin of the 3.16-MeV level was

reported by Oleksiuk et. al.[3] to be 3/2. More recently, measurements were performed at the Utrecht laboratory by Hazewindus[1] who concluded that the spin of both the resonance level and the 3.16 MeV level was 5/2. Hazewindus also performed polarization measurements and concluded that both levels were of positive parity.

Angular distributions, triple correlations, and polarization measurements have been performed in the present work at the 1214 keV and 1905 keV resonance levels. The experimental data, wherever comparisons can be made, is in excellent agreement with that reported by Hazewindus. It is observed, however, that if one considers the possibility of octupole gamma-ray mixing in the cascade through the 3.16-MeV level of Cl^{35}, the spin assignment $5/2 \rightarrow 5/2 \rightarrow 3/2$ is not unique. Spin and parity assignments of $7/2^- \rightarrow 7/2^- \rightarrow 3/2+$ will also agree with the same experimental data provided one assumes an E3/M2 mixing amplitude of -.16 in the secondary transition. Additional angular correlation measurements which were designed specifically to differentiate between these alternative spin assignments have led to the conclusion that, in fact, the 7/2 spin assignment is correct. These measurements are described following a discussion of the original and more "standard" angular correlation and polarization measurements.

5.2 Decay Scheme of the 1214 keV Resonance

Figure 5.1 shows a spectrum taken at the 1214-keV resonance with a 9" x 4" NaI(Tl) crystal, the axis of which was oriented at 55^o to the beam axis. The major components of the decay scheme are shown in Fig. 5.2. A weak gamma ray is observed at 2.34 MeV. This radiation was observed by Hazewindus and attributed to a transition to the

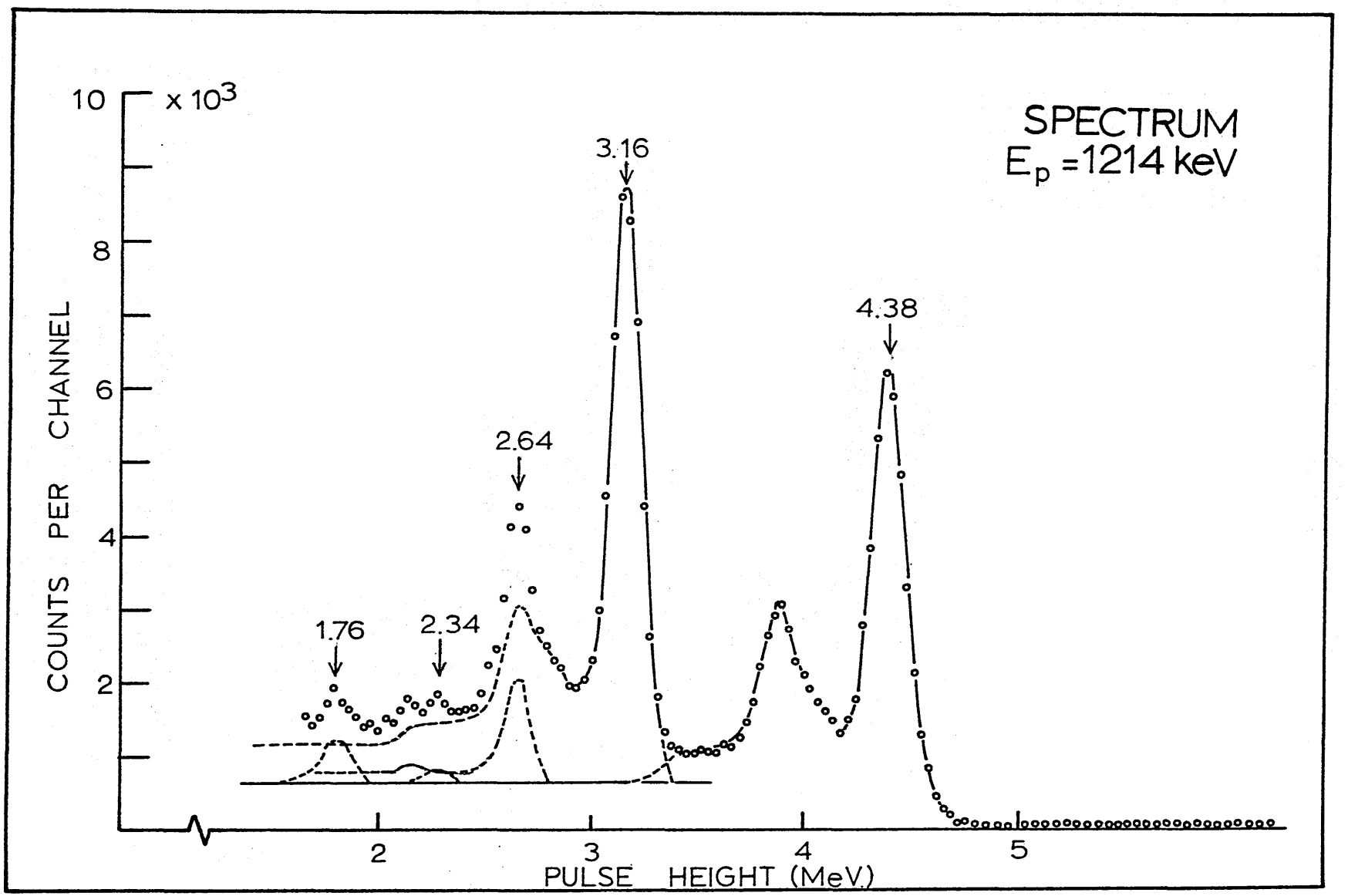
SPECTRUM
E_p =1214 keV
10
x 10^3
8
6
4
2
COUNTS PER CHANNEL
3.16
4.38
2.64
1.76
2.34
2
3
4
5
PULSE HEIGHT (MeV.)

Fig. 5.1

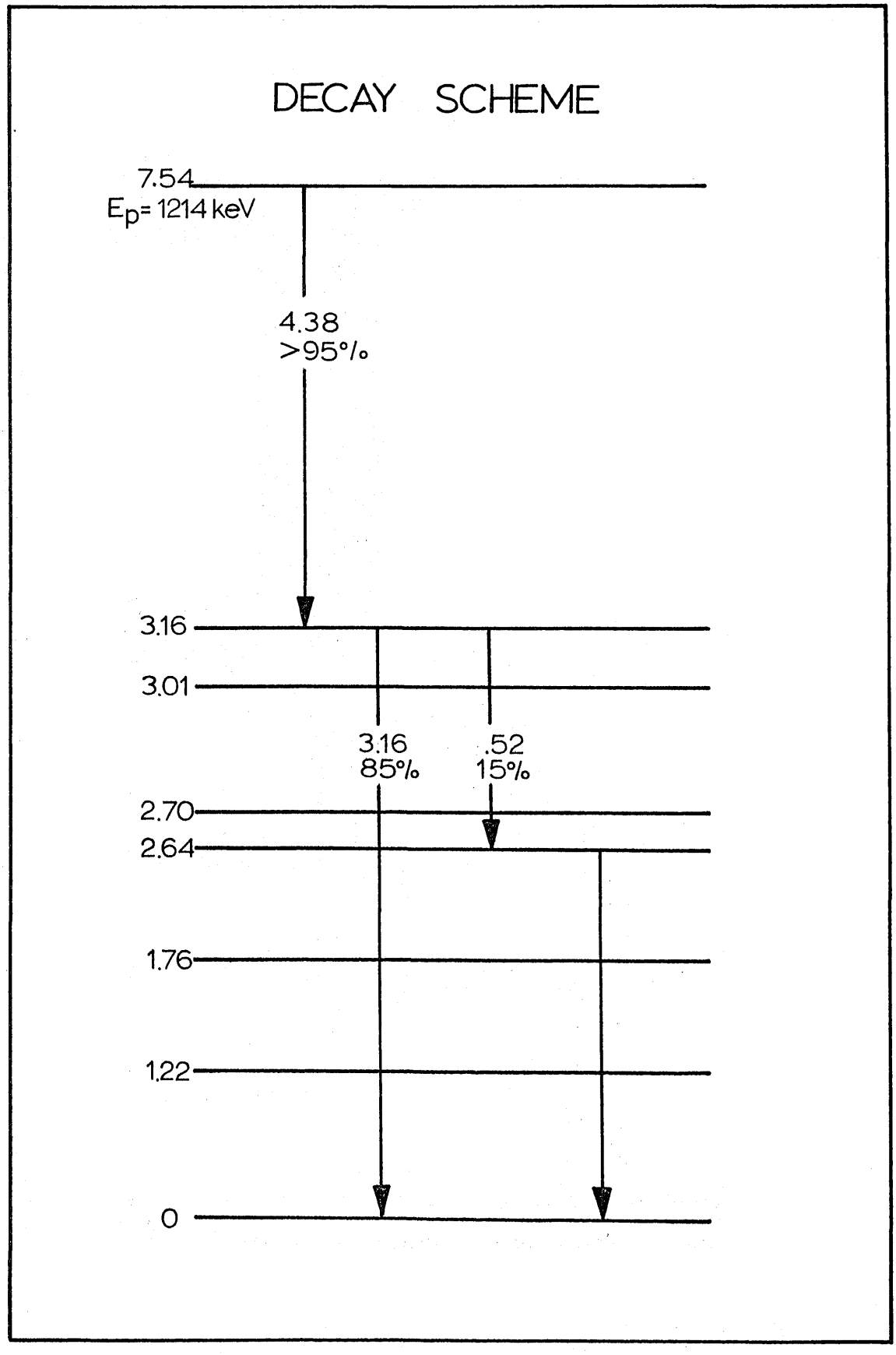
DECAY SCHEME
7.54
Ep= 1214 keV
4.38
>95%
3.16
3.01
3.16
85%
.52
15%
2.70
2.64
1.76
1.22
0

Fig. 5.2

5.22-MeV level in Cl^{35}. The 2.34-MeV gamma ray accounts for about 1% of the total radiation from the resonance level. There is also a very weak 1.76-MeV gamma ray present. This could arise from a Res.→1.76 transition where the primary gamma ray is too weak (<1.5%) to be observed in the high energy portion of the spectrum. It is also possible that part of the 1.76 MeV gamma ray results from a 3.16→1.76 transition. The very weak 1.4 MeV gamma ray, which would result from such a transition, would be difficult to observe underneath the 1.46-MeV background peak from K^{40} contained in the room walls. The 15% branching from the 3.16-MeV level to the 2.64-MeV level agrees with that reported by Hazewindus.

5.3 Angular Correlation Results from the 1214 keV Resonance

Angular distributions were measured for the primary transition (Res→3.16), and for the secondary transition (3.16→0), with the primary radiation unobserved. Triple correlations were measured in five geometries specified by the conventional θ_1, θ_2, ϕ sequence of (var, 90°, 150°), (90°, var, 180°), (var, 90°, 90°), (90°, var, 90°), and (90°, 90°, var). The variable angles were chosen to be 0°, 30°, 45°, 60°, and 90° to cover uniform steps of .25 in $\cos^2(\theta_{var})$. In the analysis of the data, all spin combinations were tried which involved J_r from 1/2 through 9/2 and $J_{3.16}$ from 1/2 through 9/2 with the restriction $\Delta J \leq 2$. The analysis was performed by a computer program which calculates values of the $\chi^2(\delta_1, \delta_2)$ surface at up to 8000 points and determines the minimum point projection or "shadow" of the surface on to both the χ^2-δ_1 plane and the χ^2-δ_2 plane. These two curves then

provide the lowest point in the χ^2 surface, the best values for δ_1 and δ_2, and the proper correlated errors in δ_1 and δ_2.

Three spin assignments were found to have reasonable minima in the corresponding χ^2 surface. They are:

5/ 2→5/ 2→3/ 2 for $\delta_1 = +.05 \pm .02, \delta_2 = -.72 \pm .02$

5/ 2→7/ 2→3/ 2 for $\delta_1 = +.49 \pm .02, \delta_2 = -.16 \pm .03$

7/ 2→7/ 2→3/ 2 for $\delta_1 = +.09 \pm .02, \delta_2 = -.14 \pm .02$

The projection contours or "shadow plots" for these three spin assignments are shown in Figs. 5.3, 5.4 and 5.5. The χ^2 value for the spin assignment 5/ 2→7/ 2→3/ 2 actually is not within the statistically allowed range. This spin sequence must, therefore, be considered as quite doubtful, but it will be kept as a possibility to be considered in the light of further measurements. The experimental data points along with the theoretical correlations for the 5/2→5/2→3/2 and for the 7/ 2→7/ 2→3/ 2 spin assignments are shown in Fig. 5.6. It is to be noted that for the two cases where $J_2 = 7/2$, acceptable solutions will be obtained only with some quadrupole-octupole mixing in the secondary transition. If gamma-ray transitions of no higher order than quadrupole are considered, then the assignment 5/2→5/2→3/2 is unique (as reported in reference 1). However, since the $J_2 = 7/2$ assignments come into quite good agreement with the experimental data for only a small amount of octupole mixing, these spin assignments are considered to merit further investigation. The next phase of the investigation consisted of performing linear polarization measurements on the two gamma rays used for the above

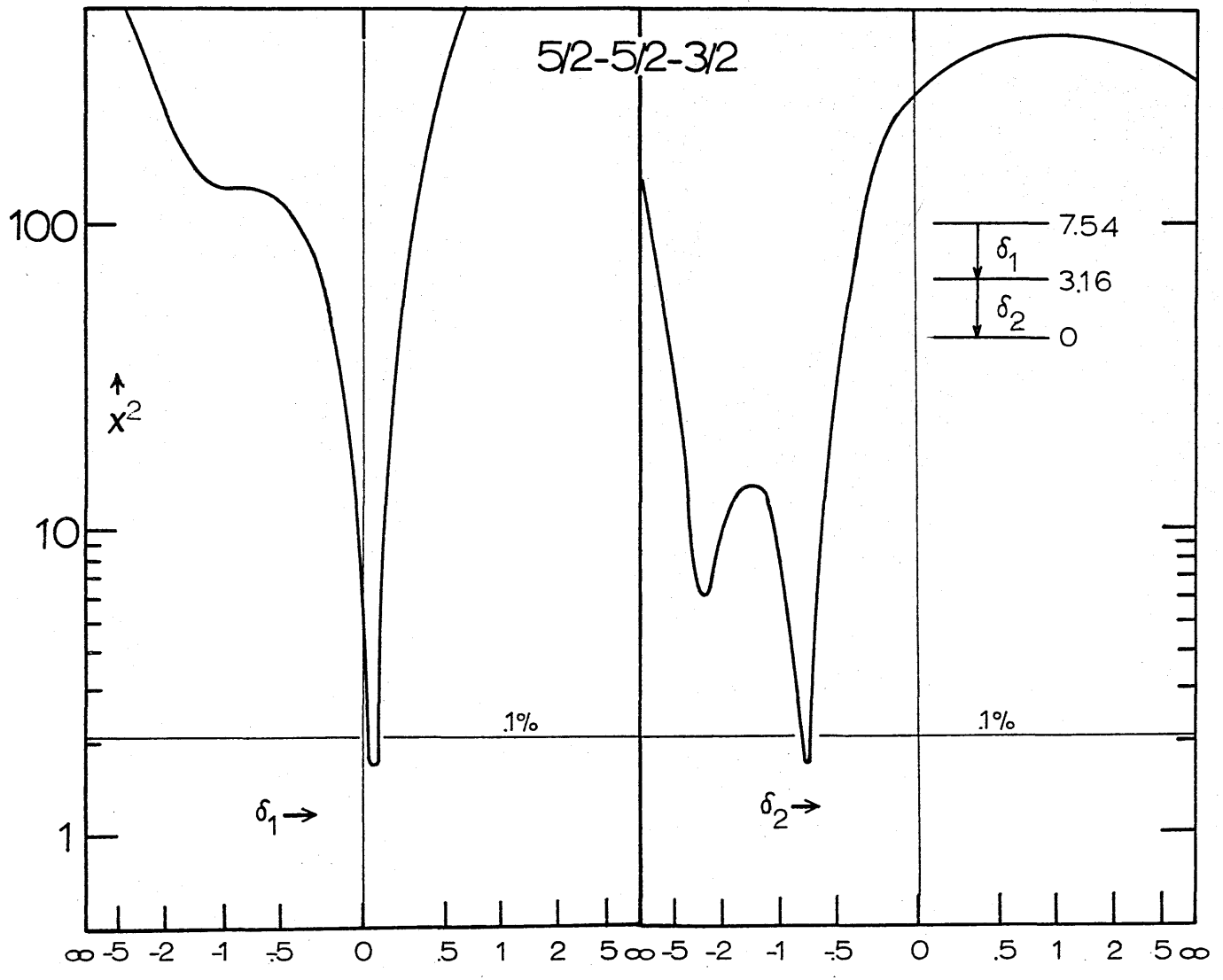
5/2-5/2-3/2
100
10
1
χ^2
.1%
.1%
δ_1→
δ_2→
7.54
δ_1
3.16
δ_2
0
∞ -5 -2 -1 -.5 0 .5 1 2 5 ∞ -5 -2 -1 -.5 0 .5 1 2 5 ∞

Fig. 5.3

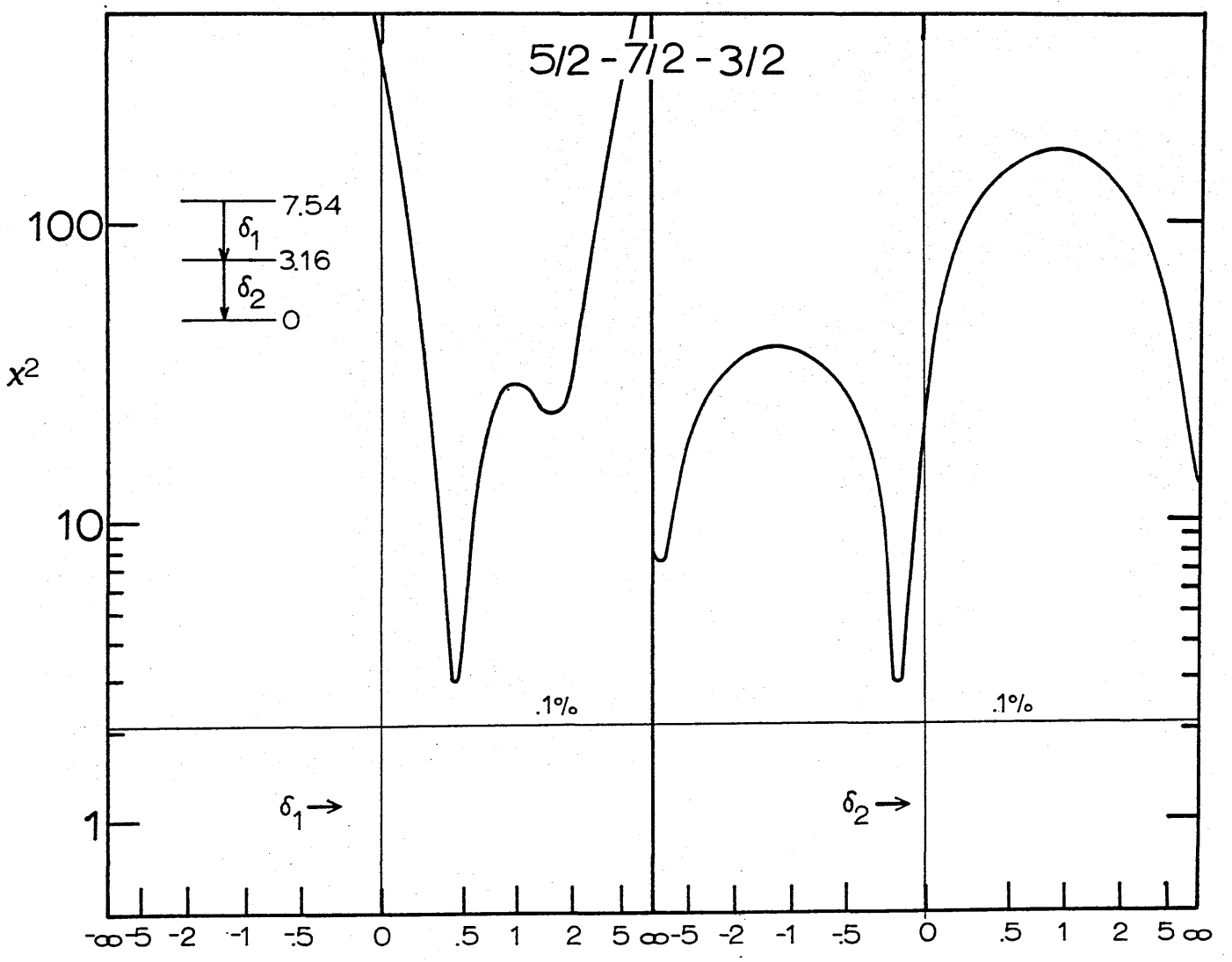
5/2 - 7/2 - 3/2
7.54
3.16
0
δ_1
δ_2
100
10
1
x^2
.1%
.1%
$\delta_1 \rightarrow$
$\delta_2 \rightarrow$
-∞ -5 -2 -1 -.5 0 .5 1 2 5 ∞ -5 -2 -1 -.5 0 .5 1 2 5 ∞

Fig. 5.4

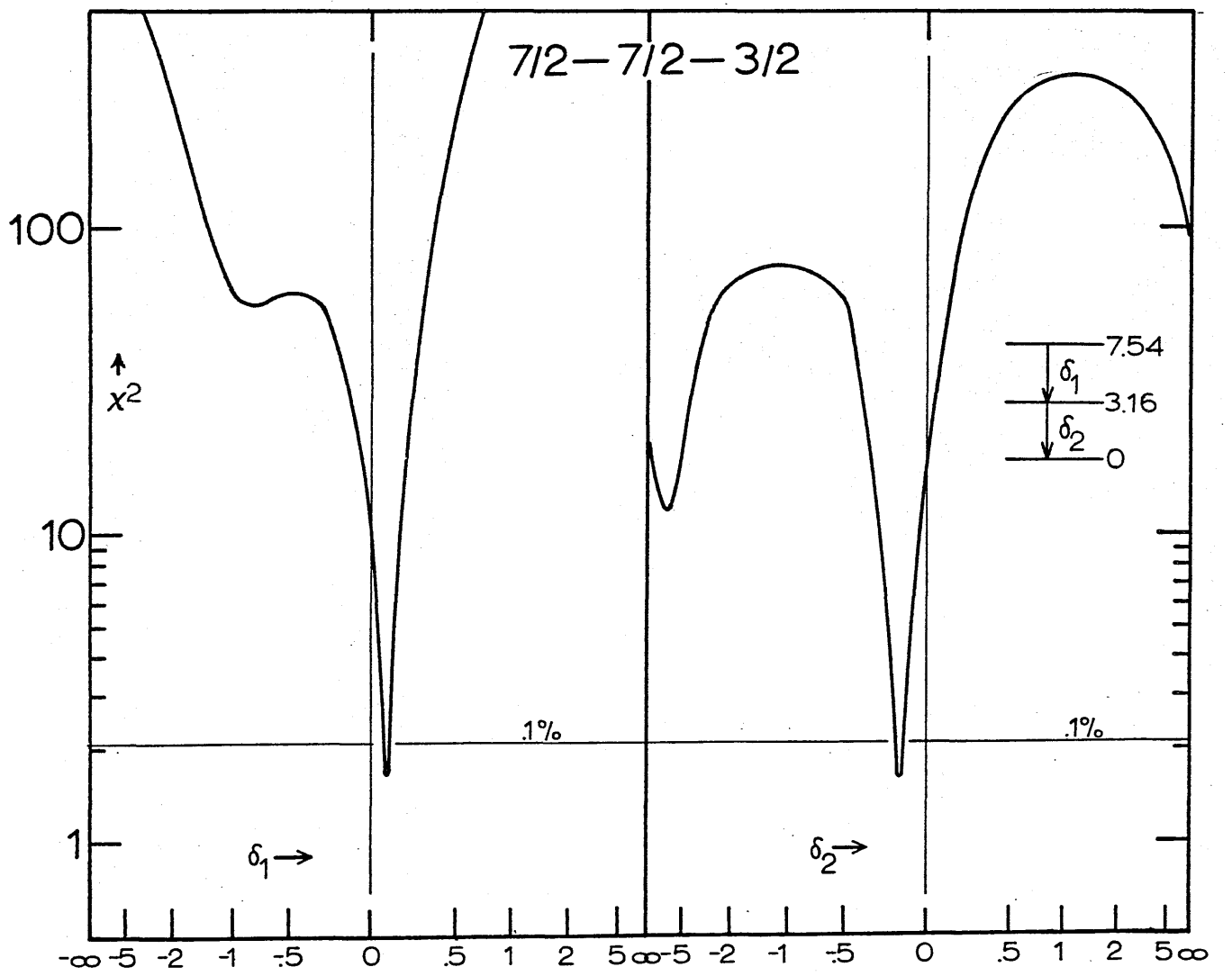
7/2−7/2−3/2
100
10
1
χ^2
.1%
.1%
$\delta_1 \rightarrow$
$\delta_2 \rightarrow$
7.54
δ_1
3.16
δ_2
0
-∞ -5 -2 -1 -.5 0 .5 1 2 5∞ -5 -2 -1 -.5 0 .5 1 2 5∞

Fig. 5.5

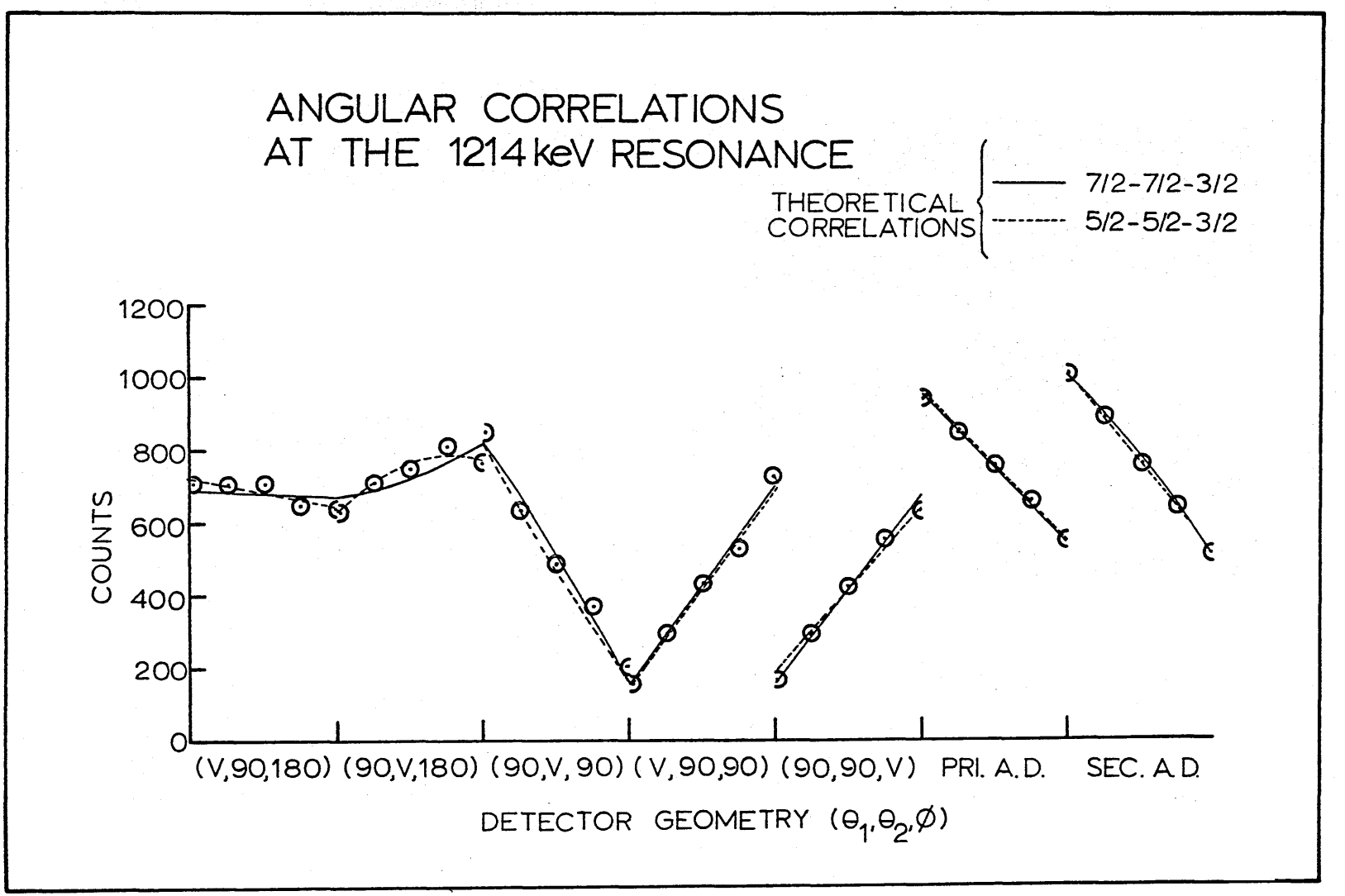
ANGULAR CORRELATIONS
AT THE 1214 keV RESONANCE
THEORETICAL CORRELATIONS
7/2-7/2-3/2
5/2-5/2-3/2
COUNTS
1200
1000
800
600
400
200
0
(V,90,180) (90,V,180) (90,V, 90) (V, 90,90) (90,90,V) PRI. A.D. SEC. A.D.
DETECTOR GEOMETRY (θ1,θ2,Ø)

Fig. 5.6

directional correlation measurements.

5.4 Polarization Measurements at the 1214 keV Resonance

The linear polarizations of the gamma rays of both the Res.→3.16 and 3.16→0 transitions have been measured with a Compton polarimeter, built by Dr. F. W. Prosser of this laboratory. Electronic summing of the coincident pulses between the scattering and absorbing crystals was incorporated so as to increase the energy resolution of the device. The polarization measurement yielded the intensity ratio of gamma rays scattered vertically to those scattered horizontally from a 1" x 1" NaI crystal set in the horizontal plane at 90° to the incident proton beam. This gamma-ray intensity ratio is denoted by $\frac{N_o}{N_{90}}$ and can be calculated as a function of the spins, multipolarity mixing ratios, and parity of the gamma-radiations[4,5]. Since the mixing ratios for each possible spin assignment have already been determined by the directional correlations, the theoretical value of $\frac{N_o}{N_{90}}$ can be predicted uniquely for each assumed spin and parity. The experimental results were:

Primary Transition: $= .76 \pm .05$

Secondary Transition: $= 1.27 \pm .1$

As stated earlier, three spin combinations are of interest: 5/2→5/2→3/2, 5/2→7/2→3/2, and 7/2→7/2→3/2. In Figs. 5.7 and 5.8 the theoretical values for $\frac{N_o}{N_{90}}$ are plotted versus arctan δ_1 for the primary transition. The vertical bars are the measured values of δ_1 and the horizontal bar represents the measured value of $\frac{N_o}{N_{90}}$. Agreement is obtained in the following cases:

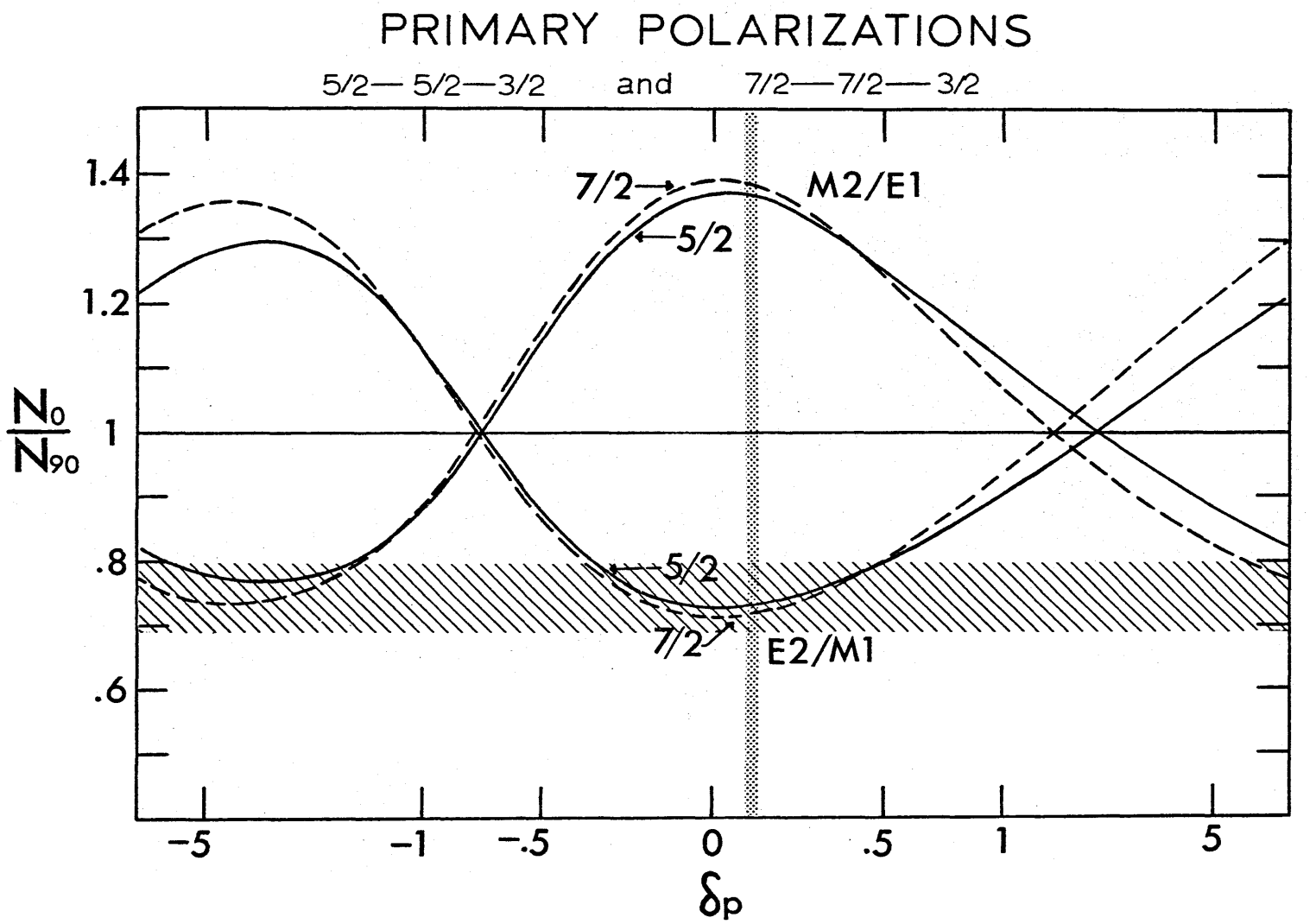
PRIMARY POLARIZATIONS
5/2— 5/2—3/2 and 7/2—7/2—3/2
1.4
1.2
1
.8
.6
N0/N90
7/2
M2/E1
5/2
5/2
7/2
E2/M1
−5
−1
−.5
0
.5
1
5
δp

Fig. 5.7

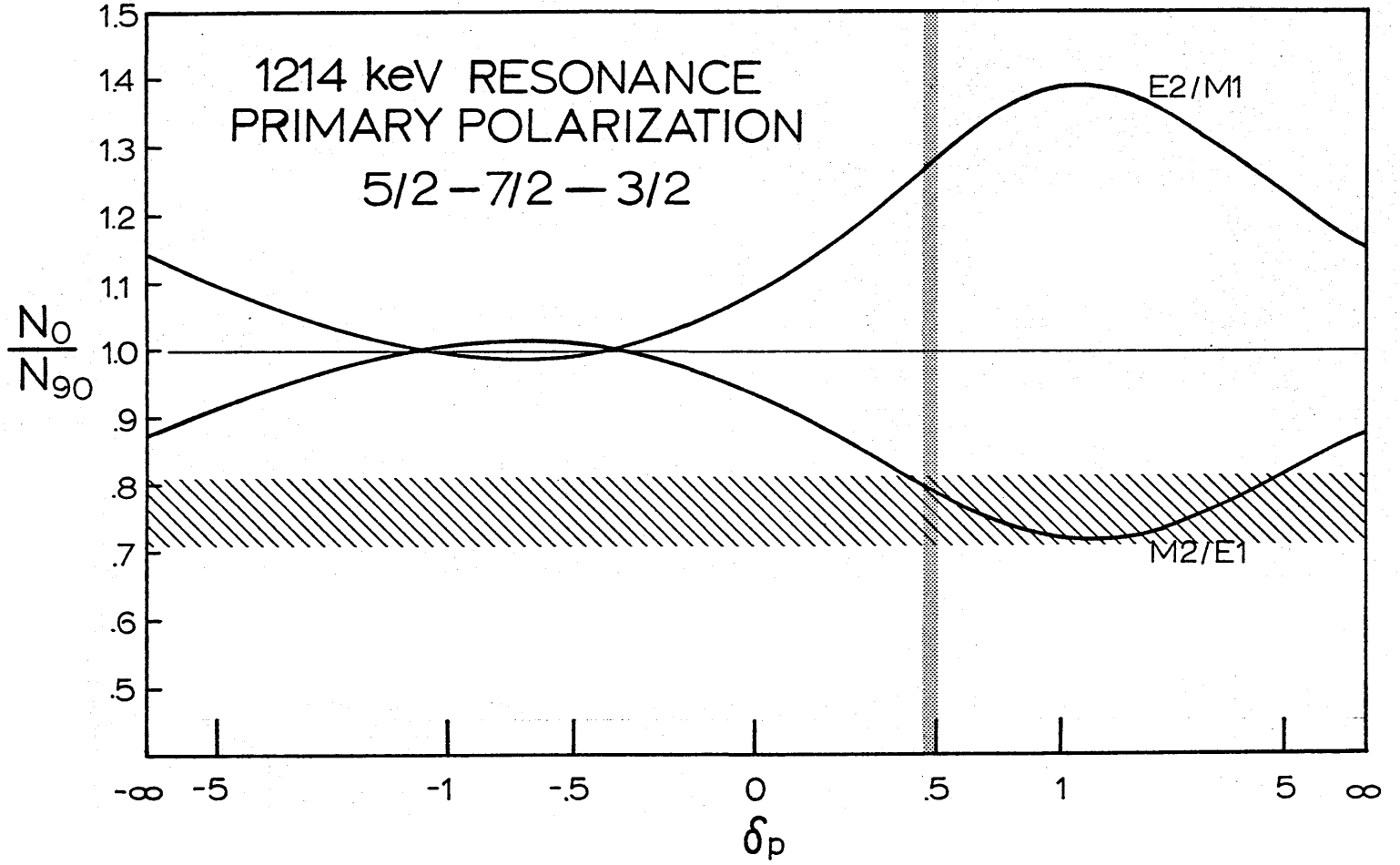
1214 keV RESONANCE
PRIMARY POLARIZATION
5/2 – 7/2 – 3/2
E2/M1
M2/E1
N0/N90
1.5
1.4
1.3
1.2
1.1
1.0
.9
.8
.7
.6
.5
-∞
-5
-1
-.5
0
.5
1
5
∞
δp

Fig. 5.8

$J_{Res.}$	Radiation Type	$J_{3.16}$
5/2	E2/M1	5/2
5/2	M2/E1	7/2
7/2	E2/M1	7/2

The spin assignment 5/2→7/2→3/2 requires an M2/E1 amplitude ratio of .49. This amount of M2/E1 mixing, along with the observed resonance strength of $\omega\gamma \approx 2$eV, implies an M2 transition strength of 10^3 Weisskopf units. This M2 strength is too large for either theoretical explanation or experimental precendent. The 5/2→7/2→3/2 spin assignment was also in poor agreement with the directional correlation measurements and, therefore, it will now be ruled out as incorrect. The secondary gamma-ray polarization curves for the remaining two possible spin assignments are shown in Fig. 5.9. These polarization curves are the same as the polarization curves for the primary transition except that these secondary polarization curves are calculated for the fixed measured value of the primary mixing parameter since the value of $\frac{N_o}{N_{90}}$, in this case, depends on both primary and secondary mixing parameters. The results of the polarization measurements are summarized below:

$J^{\pi}_{Res.}$		mixing		$J^{\pi}_{3.16}$		mixing		J^{π}_{o}
5/2+	-	M1/E2 = .05	-	5/2+	-	M1/E2 = -.72		-3/2+
7/2-	-	M1/E2 = .09	-	7/2-	-	M2/E3 = -.14		-3/2+

5.5 Measurements at the 1905 keV Resonance

The resonance at Ep = 1905 keV has been observed by Yang Tan[11]. He noted that this resonance cascades strongly through the

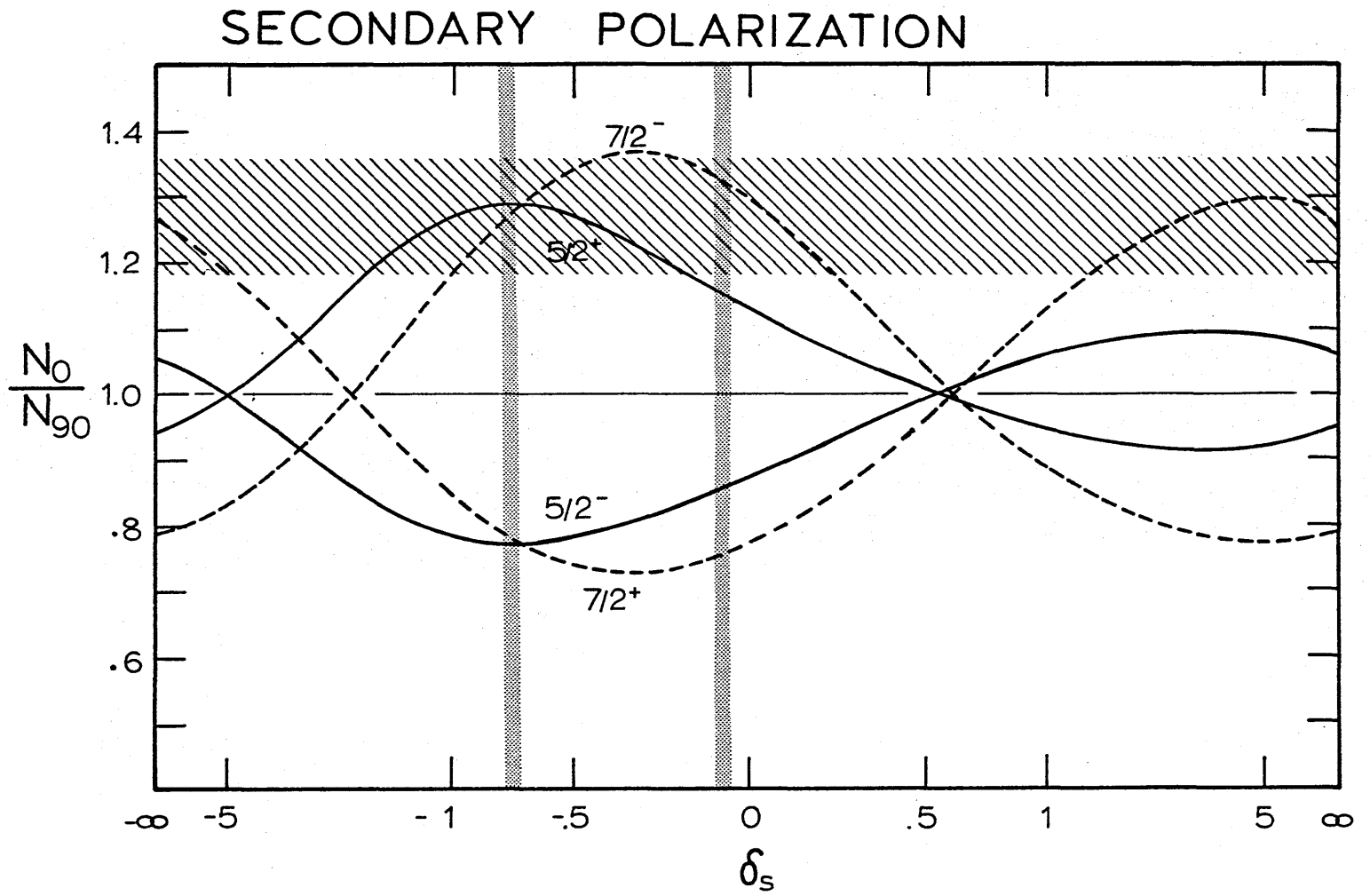
SECONDARY POLARIZATION
1.4
1.2
1.0
.8
.6
$\frac{N_0}{N_{90}}$
7/2⁻
5/2⁺
5/2⁻
7/2⁺
-∞
-5
-1
-.5
0
.5
1
5
∞
δ_s

Fig. 5.9

3.16 MeV level and has, in addition, a transition to the ground state. The spectrum at this resonance is shown in Fig. 5.10 and the decay scheme and branching ratios are shown in Fig. 5.11. The results of the analysis of the angular distribution of the ground state gamma transition are shown in Fig. 5.12. Acceptable solutions can be obtained for both $J_r = 3/2$ with $\delta = .73 \pm .03$ or $\delta = 2.6 \pm .15$ and for $J_r = 5/2$ with $\delta = .05 \pm .02$. Then, since the spin of the 3.16-MeV level has already been limited to either 5/2 or 7/2, the only remaining possibilities for the spin sequence of the Res→3.16→0 cascade are: 3/2→5/2→3/2, 3/2→7/2→3/2, 5/2→5/2→3/2, and 5/2→7/2→3/2. Angular distribution and triple correlation data from the Res→3.16→0 cascade have been analyzed for the four possible spin sequences and the results are shown in Figs. 5.13 and 5.14. The data used in the analysis is shown in Fig. 5.15. Solutions are obtained for:

	$J_{8.22}$	$J_{3.16}$	J_o	δ_1	δ_2
1.	3/2	5/2	3/2	$-.10 \pm .02$	$-.70 \pm .04$
2.	3/2	5/2	3/2	$-.10 \pm .02$	$-2.9 \pm .02$
3.	5/2	7/2	3/2	$-.02 \pm .02$	$-.15 \pm .02$

The second solution for $\delta_2 = -2.9$ is ruled out by the experiments at the 1214-keV resonance, but the other two solutions agree with the previous results of $J_{3.16} = 5/2$ with $\delta_2 = -.7$ or $J_{3.16} = 7/2$ with $\delta_2 = -.14$. Thus, even though the two resonances have different spins and different decay modes, the same 5/2→7/2 ambiguity of the spin of the 3.16-MeV level persists in both resonances. At the 1905-keV resonance, the

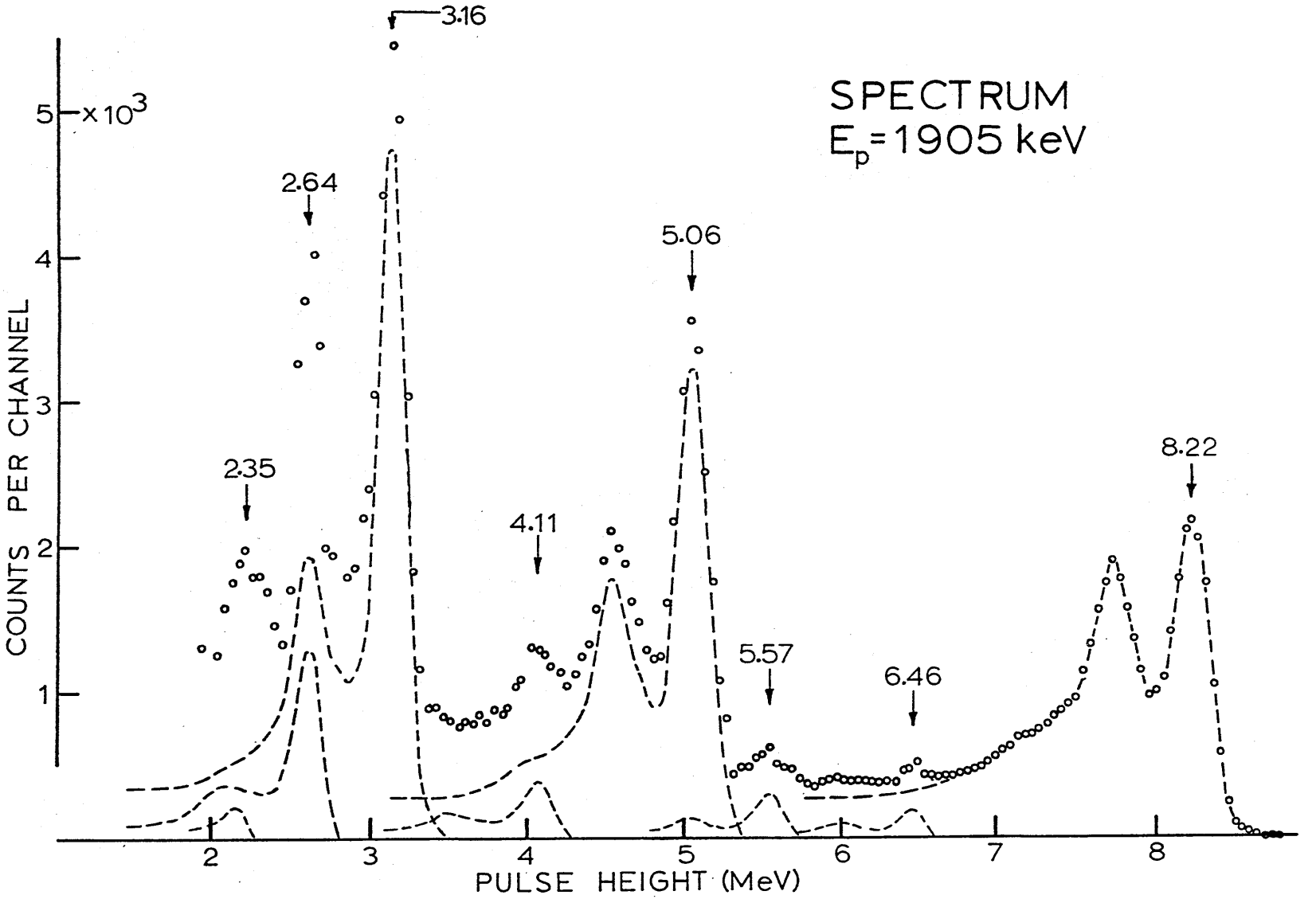
SPECTRUM
E_p=1905 keV
3.16
2.64
5.06
2.35
4.11
8.22
5.57
6.46
x10^3
COUNTS PER CHANNEL
PULSE HEIGHT (MeV)
1
2
3
4
5
2
3
4
5
6
7
8

Fig. 5.10

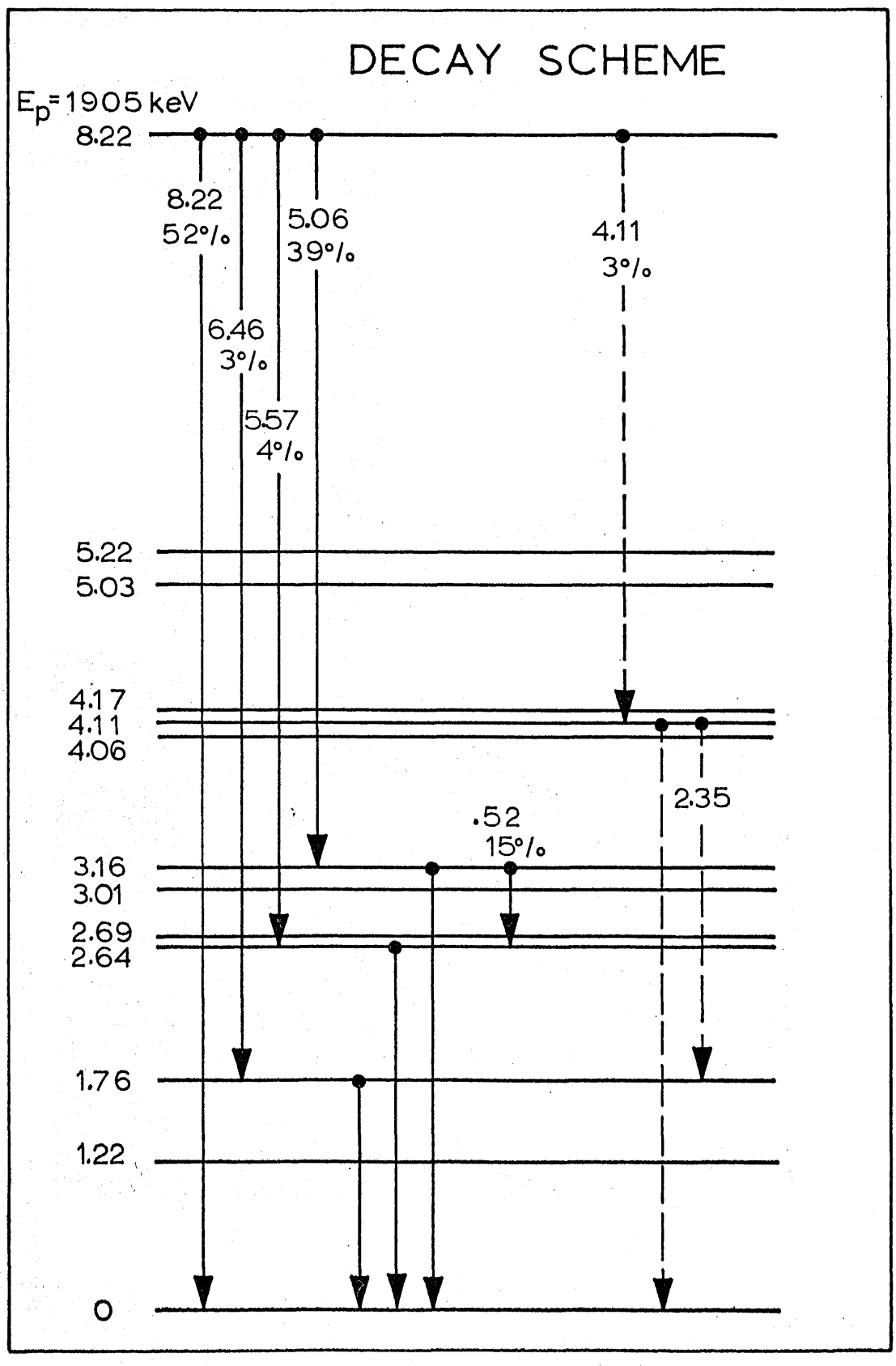
DECAY SCHEME
E_p = 1905 keV
8.22
5.22
5.03
4.17
4.11
4.06
3.16
3.01
2.69
2.64
1.76
1.22
0
8.22
52%
6.46
3%
5.57
4%
5.06
39%
4.11
3%
.52
15%
2.35

Fig. 5.11

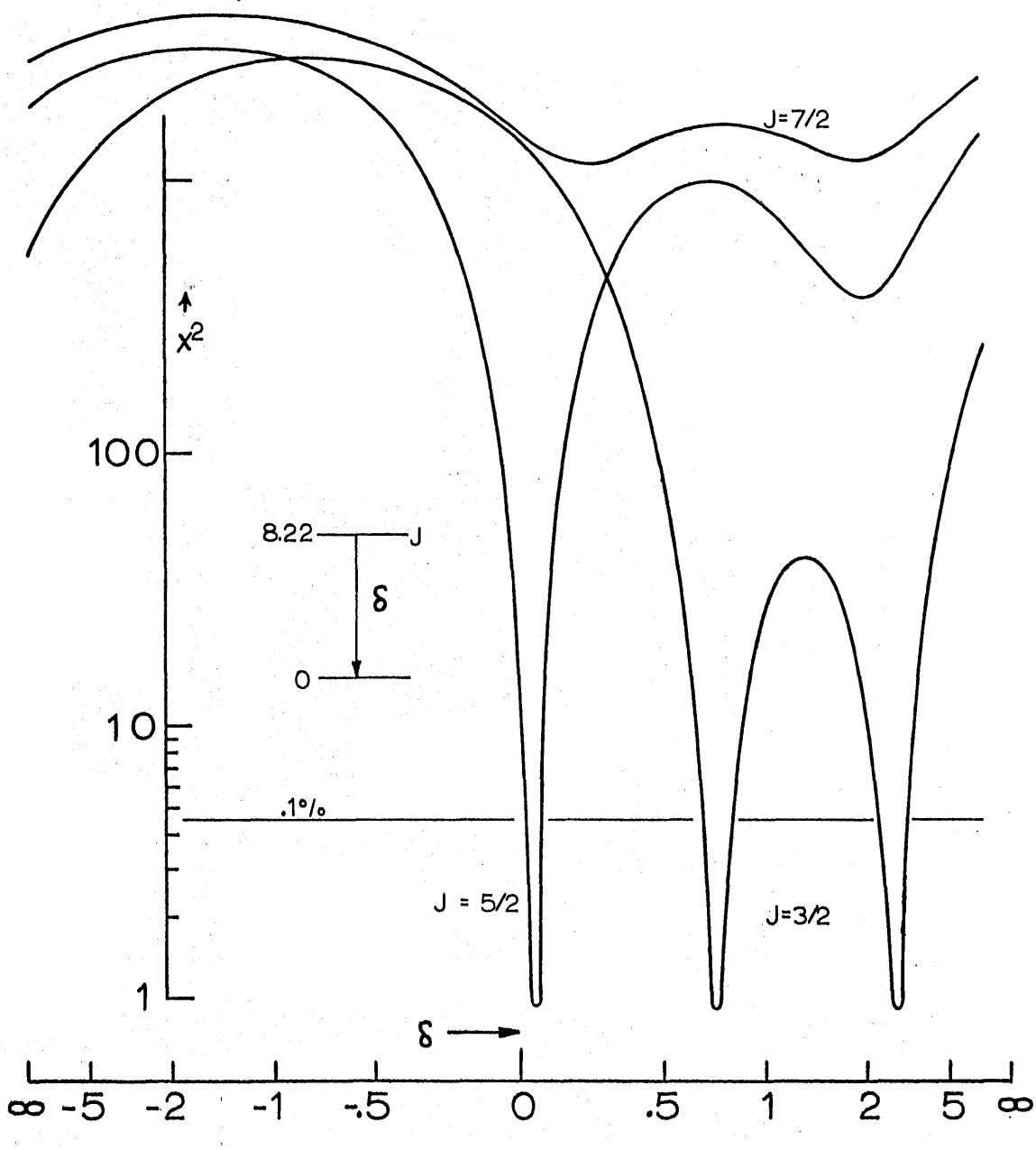

Fig. 5.12

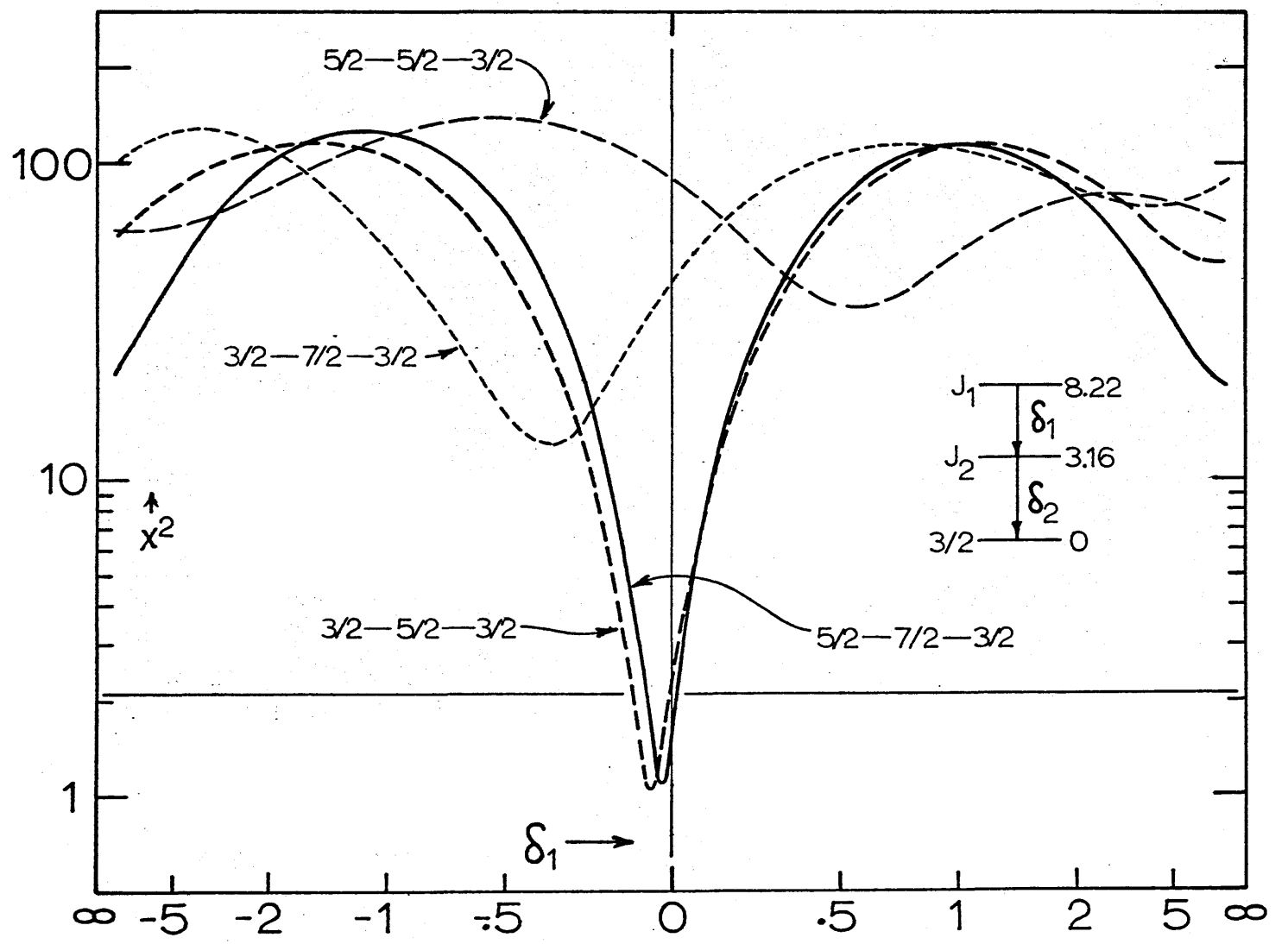
5/2—5/2—3/2
3/2—7/2—3/2
3/2—5/2—3/2
5/2—7/2—3/2
100
10
1
χ^2
δ_1
J_1 8.22
δ_1
J_2 3.16
δ_2
3/2 0
∞ -5 -2 -1 -.5 0 .5 1 2 5 ∞

Fig. 5.13

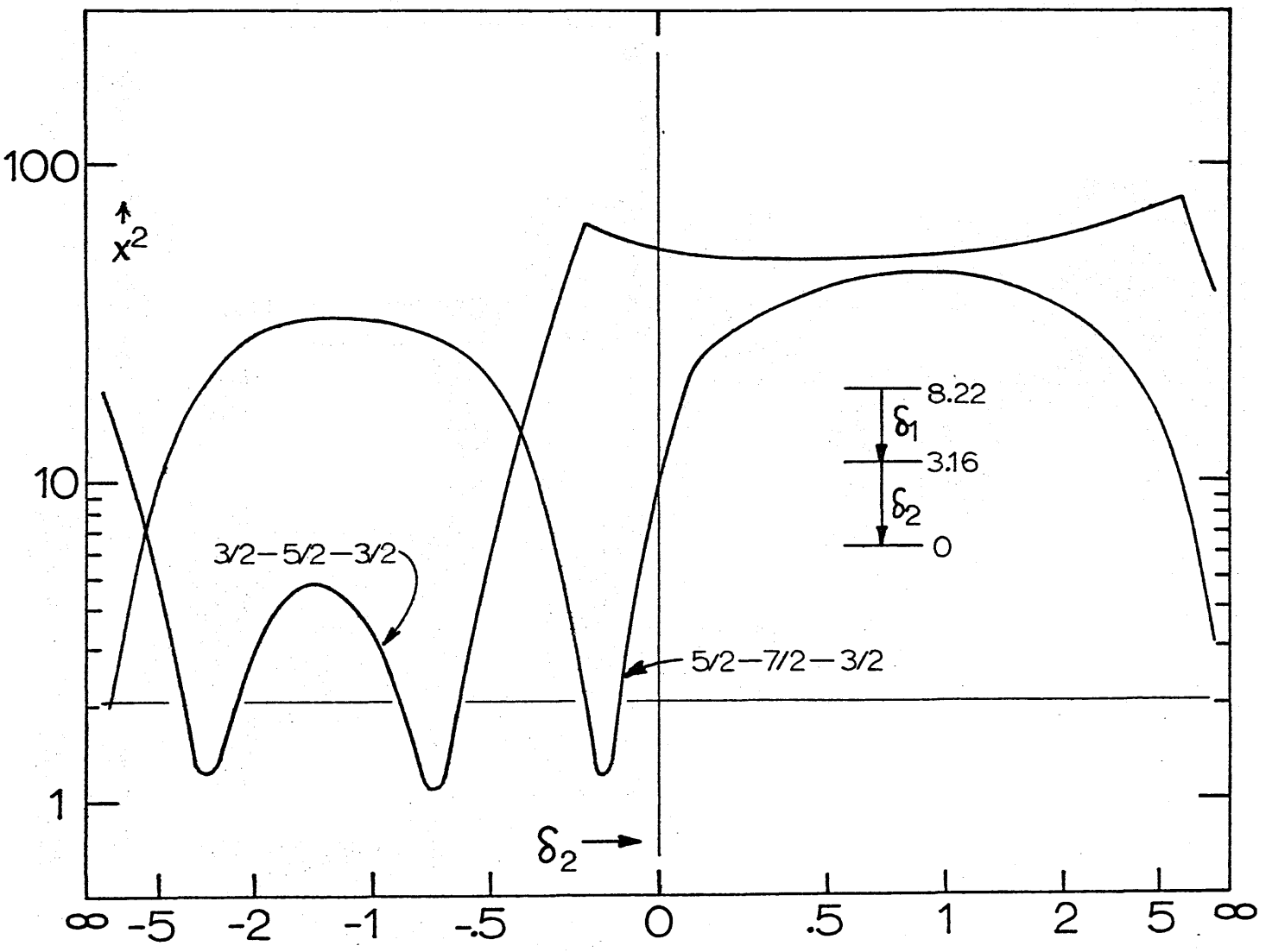
100
10
1
χ^2
3/2–5/2–3/2
5/2–7/2–3/2
8.22
δ_1
3.16
δ_2
0
δ_2
∞ -5 -2 -1 -.5 0 .5 1 2 5 ∞

Fig. 5.14

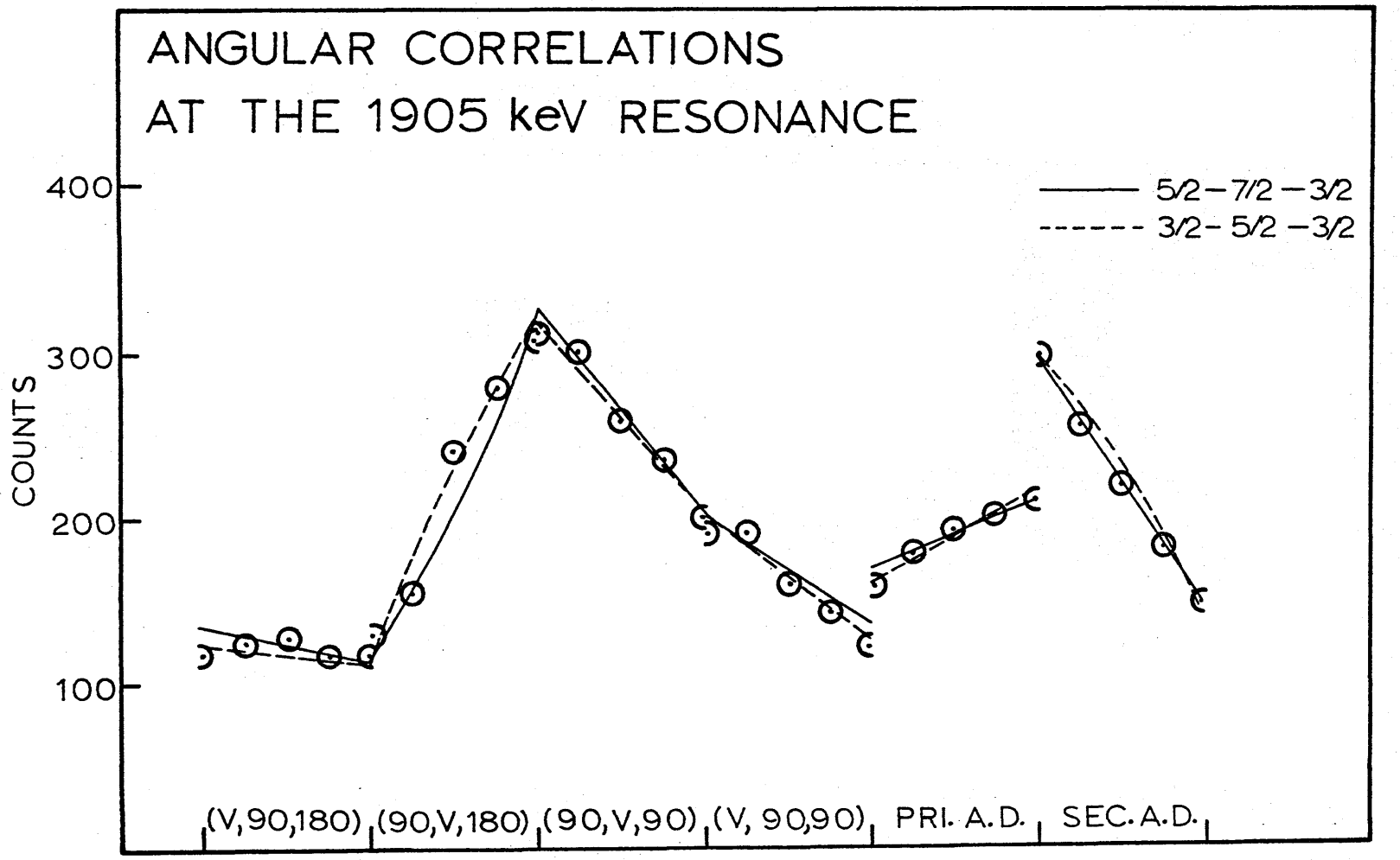
ANGULAR CORRELATIONS
AT THE 1905 keV RESONANCE
5/2 – 7/2 – 3/2
3/2 – 5/2 – 3/2
COUNTS
400
300
200
100
(V,90,180)
(90,V,180)
(90,V,90)
(V, 90,90)
PRI. A.D.
SEC. A.D.

Fig. 5.15

theoretical angular correlation functions for the two alternative spin assignments are so nearly identical that directional correlation measurements are inadequate to choose between the two possible assignments. Neither will a linear polarization measurement provide the correct spins since the mixing parameters are such as to produce nearly the same scattering asymmetry ratio for either spin sequence. Fortunately the prospects for making additional measurements in order to learn the correct spin of the 3.16 level, and consequently the spins of both resonance levels, appear brighter at the 1214-keV resonance.

5.6 Additional Angular Correlation Measurements at the 1214 keV Resonance

As can be seen in Fig. 5.6, the theoretical curves for the 5/2 spin assumption differ somewhat from the theoretical curves for the 7/2 spin assumption over some of the sets of angles at which measurements were performed, but the curves are not significantly different for other sets of angles. The possibility is indicated, therefore, of selecting a particular set of angles over which the difference between the spin 5/2 and spin 7/2 correlations are sufficiently large so as to be distinguished by an accurate triple correlation measurement. A search for a good set of angles revealed that the (90°, var, 180°) configuration was close to optimum but that some additional difference between the 5/2 and 7/2 correlations would be introduced via an X^1_{22} term which contributes to the correlation function when the fixed angle θ_1 is moved somewhat away from 90°. These considerations, together with considerations of the mechanical symmetry of the experimental apparatus, lead to a

choice of the set (120°, var, 180°). Additional very important information could be obtained if the absolute normalization of the data points could be measured. In order to establish a normalization, the angles chosen for the correlation measurement were extended to include a set over which the theoretical curves for 5/2 and 7/2 were nearly identical. Since the correlation measurements over this set of angles were independent of which spin is correct, they could be used to establish the normalization and to calibrate the experimental apparatus. This phase of the correlation measurement covered the set (var, 90°, 180°) where the variable angle, θ_1, ran from 90° to 135°. The angles covered in the experiment are shown in Fig. 5.16. Measurements were performed at angles corresponding to steps of .1 in $\cos^2\theta_{var}$ except near the end point around (120°, 0°, 180°) where the theoretical curves were changing rapidly and some steps of .05 in $\cos^2\theta_{var}$ were included. The data obtained, after having been corrected for gamma ray absorbtion by the target backing and target chamber, is shown in Fig. 5.17. The data points shown are averages of from three to six individual measurements. A total of over 80 such measurements were performed for the single composite-geometry. The two curves shown in Fig. 5.17 are the theoretical correlation curves for the 5/2→5/2→3/2 and for the 7/2→7/2→3/2 spin sequence calculated using values for the mixing parameters as determined from the previous correlation measurements. The χ^2 values for these two curves are 3.4 and .93 respectively. For this last correlation measurement alone, a better fit can be obtained for the 5/2 assignment by allowing the primary mixing parameter to have the value $\delta_1 = -.09 + .02$

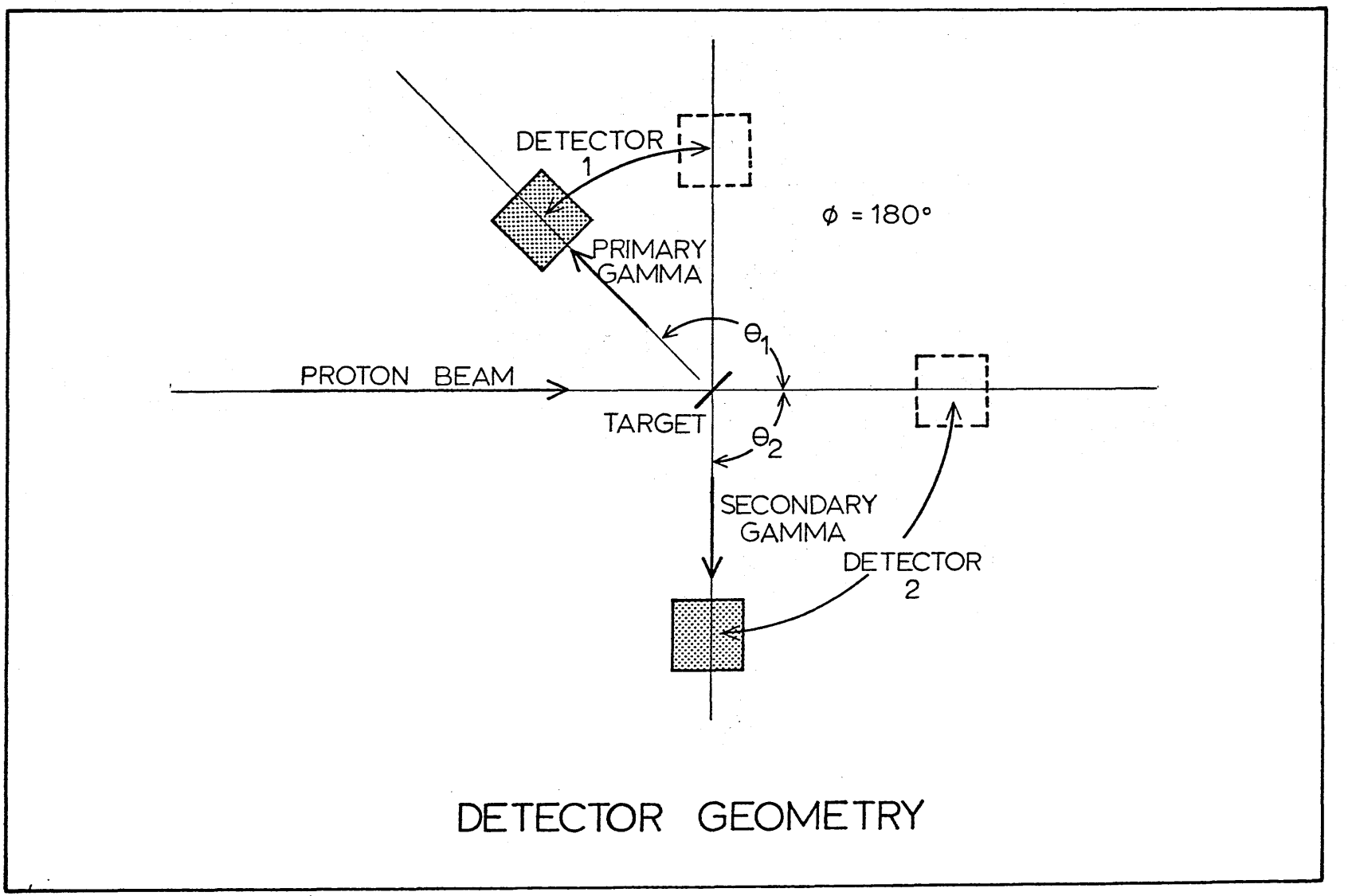
DETECTOR
1
φ = 180°
PRIMARY
GAMMA
θ1
PROTON BEAM
TARGET
θ2
SECONDARY
GAMMA
DETECTOR
2
DETECTOR GEOMETRY

Fig. 5.16

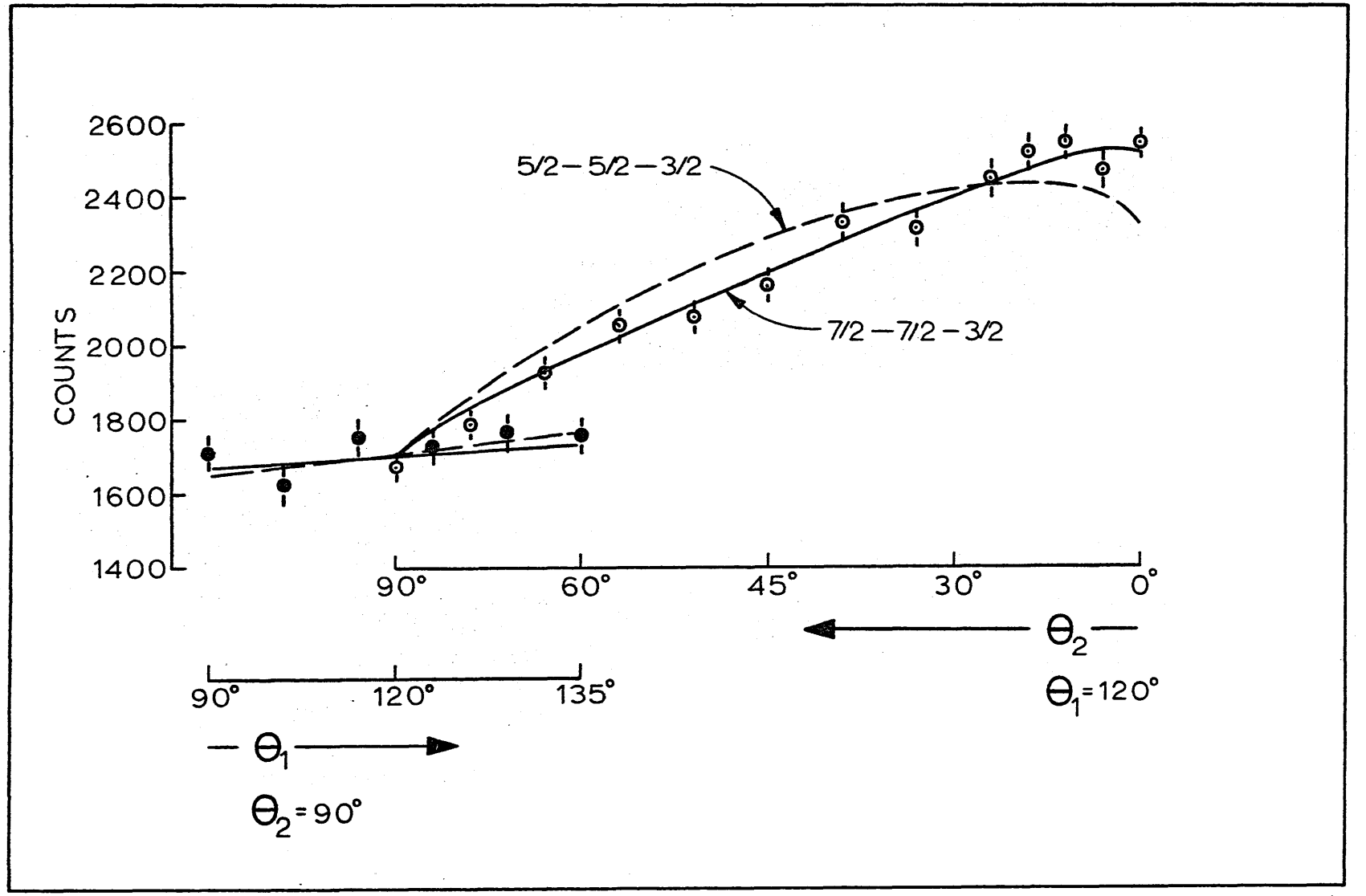
2600
2400
2200
2000
1800
1600
1400
COUNTS
5/2 – 5/2 – 3/2
7/2 – 7/2 – 3/2
90°
60°
45°
30°
0°
θ2
θ1=120°
90°
120°
135°
θ1
θ2=90°

Fig. 5.17

rather than + .05 ± .02 as previously measured. (The χ^2 value drops to 1.7 in this case.) The extent to which this discrepancy is significant can be easily determined by including data from the previous correlation measurements along with this last measurements. The χ^2 curves from the computer analysis of the full set of data are shown in Figs. 5.18 and 5.19. The theoretical correlations obtained from this analysis are shown in Fig. 5.20 for (120^o, var, 180^o) configuration and also for the parimary angular distribution. The slightly negative primary mixing ratio which was required to obtain the best agreement in the (120^o, var, 180^o) geometry for the spin 5/ 2 case, and the slightly positive value for the primary mixing necessary to produce agreement with the angular distribution, cannot be satisfactorily compromised. The data is, however, all consistent with the hypothesis of 7/ 2→7/ 2→3/ 2, δ_1 = .09 ± .02, δ_2 = -.16 ± .02.

5.7 Discussion

We conclude the following:

Levels	Spin (Parity)	Mixing Amplitude
8.22 - 0	5/ 2 - 3/ 2+	+ .05 ± .02
8.22 - 3.16	5/ 2 - 7/ 2-	- .02 ± .02
5.45 - 3.16	7/ 2⁻ - 7/ 2-	+ .07 ± .02
3.16 - 0	7/ 2⁻ - 3/ 2+	- .16 ± .01

In cases where more than one independent measurement of the mixing ratio was made, the above result in a weighted average.

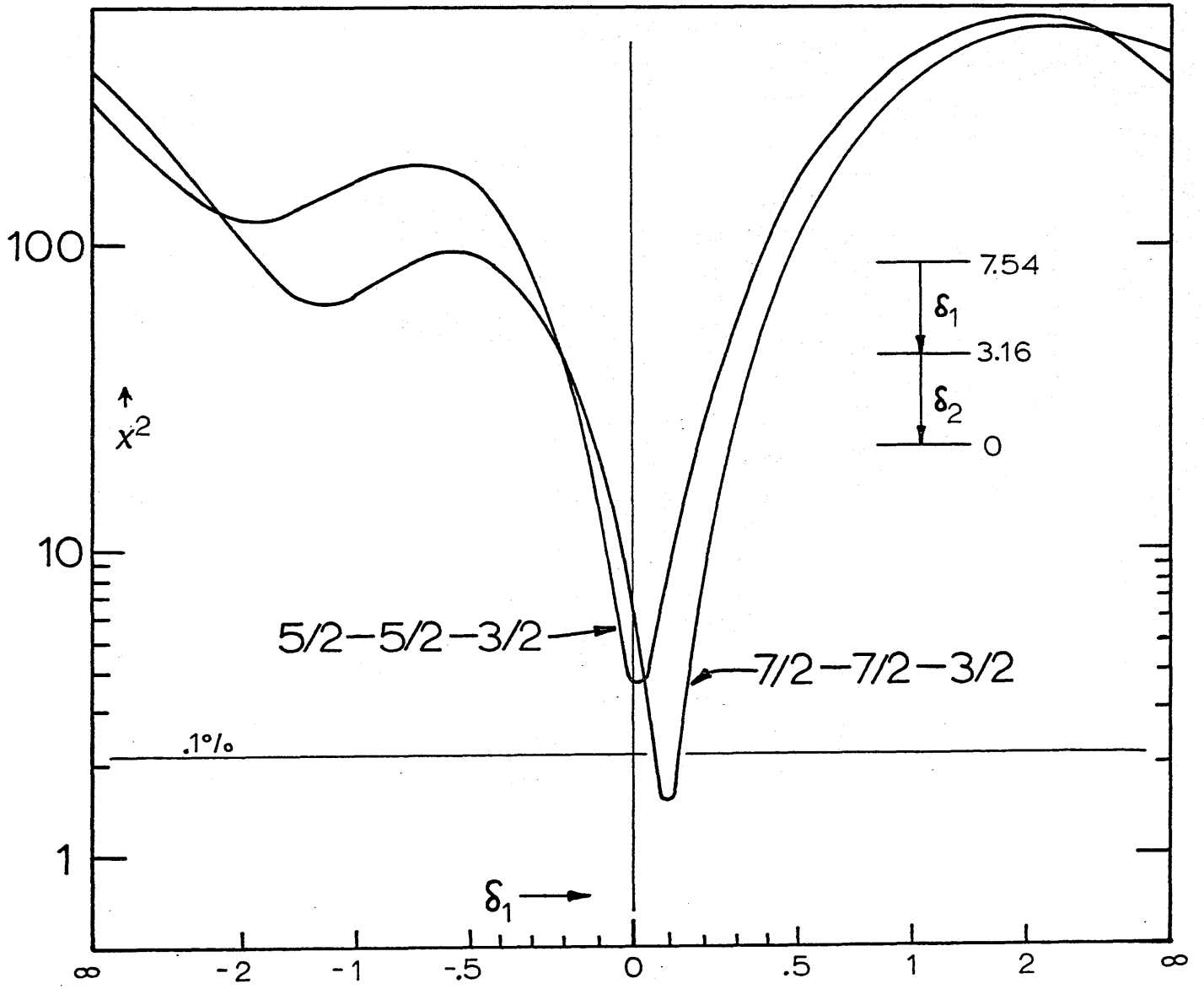
100
10
1
x^2
7.54
δ_1
3.16
δ_2
0
5/2−5/2−3/2
7/2−7/2−3/2
.1%
δ_1
∞
-2
-1
-.5
0
.5
1
2
∞

Fig. 5.18

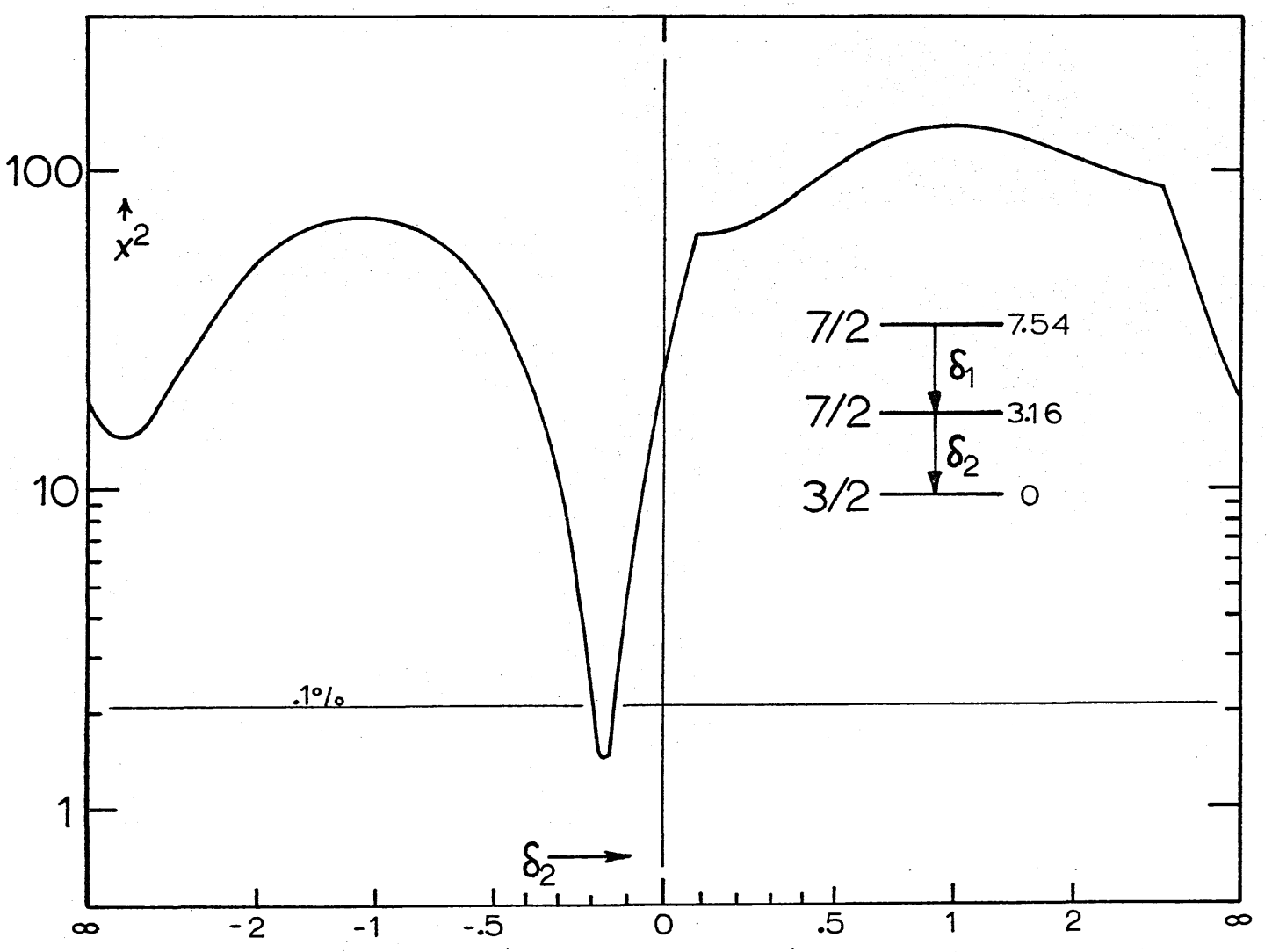

Fig. 5.19

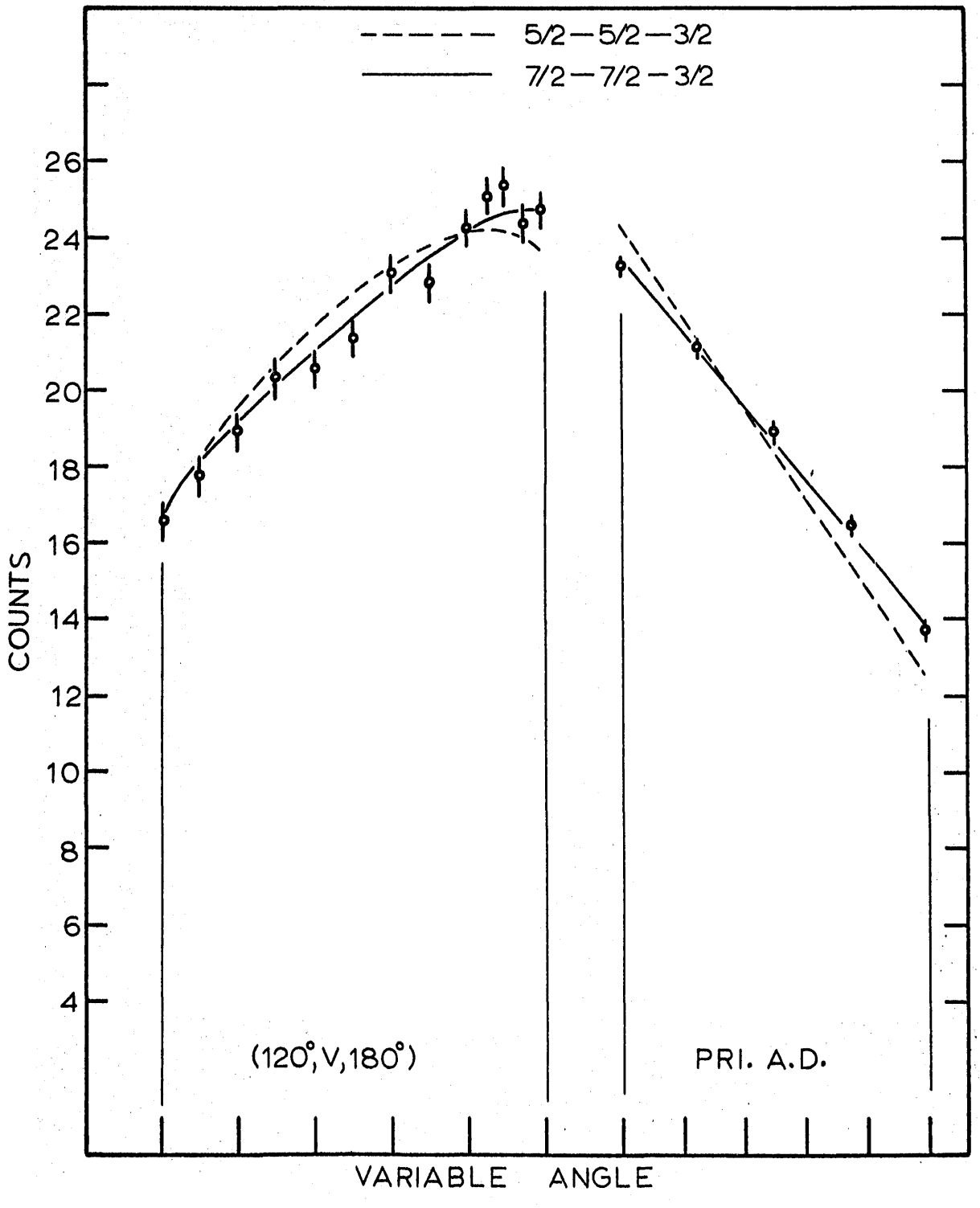
5/2−5/2−3/2
7/2−7/2−3/2
26
24
22
20
18
16
14
12
10
8
6
4
COUNTS
(120°,V,180°)
PRI. A.D.
VARIABLE ANGLE

Fig. 5.20

In view of the assignment 7/2- to the 7.54 MeV and 3.16 MeV levels, the absence of a strong transition from either of these levels to the 5/2+ level at 1.76 MeV is notable. Perhaps this E1 inhibition can result from the rather complex configuration which seems necessary to explain the properties of the 5/2+ level. It is, of course, tempting to speculate that these 7/2- levels are due to the $f_{7/2}$ orbital which is available to an outer nucleon in Cl^{35}. The large resonance width ($\omega\gamma \approx 2$eV) of the 1214-keV resonance indicates that the strength of the M1 transition to the 3.16 MeV level from the 7.54 MeV level is about .3 Weisskopf units. The measured E3/M2 intensity ratio for the 3.16→0 transition is 2.9×10^{-2}. Weisskopf estimates yield an E3/M2 ratio of about 2×10^{-3}. Thus, if one assumes an M2 strength of from .1 to 1 Weisskopf units,* one has a corresponding E3 strength of from 1.5 to 15 Weisskopf units.

In connection with this discussion of the E3/M2 transition in Cl^{35}, it is interesting to note a recent observation by P. Kossanyi-Demay et. al.[6] Using high energy electron scattering, they observed an E3 excitation of the 7/2- level at 4.43 MeV in P^{31}. The measured transition strength of the E3 excitation was 4.2 Weisskopf units. An electric octupole excitation of the 1.35-MeV level in F^{19} has also been measured from coulomb scattering studies by Litherland et. al.[7] In this case, the transition strength is 12 Weisskopf units. A mixed E1, M2, E3 transition in N^{14} has been reported by Blake et. al.[8]; and in Si^{28} a probable E3 transition has very recently been observed by Nordhagen[9]. Thus, it appears that enhanced E3 transitions are being established in this mass region.

*A few measurements in s-d shell nuclei have yielded M2 transition strengths of this order; otherwise the choice is arbitrary and only for the sake of comparing the M2 and E3 mixing.

It is also interesting to compare the resonance at 1214 keV in $S^{34}(p,\gamma)Cl^{35}$ with the resonance at 2187 keV in $Si^{30}(p,\gamma)P^{31}$ observed by Harris et. al.[10] which feeds the above mentioned 4.43 MeV level in P^{31}. Both resonances are the strongest in the energy range up to at least 2.2 MeV; both resonances are 7/2-; and both decay almost entirely to 7/2- levels via an M1 transition with very slight positive E2 mixing. This data, along with the enhanced E3 transitions mentioned above, results in a striking similarity.

References from Section 5

1. Hazewindus, N., Thesis, Delft, Netherlands. (1964).

2. Antuvjev, Yu. P., Valter, A. K., Gonchar, V. Yu., Kopanets, E. G., Livov, A. N. and Tsytko, S. P., Izvest. Akad. Navk. S.S.S.R., Ser. Fiz. 25 (1961) 265.

3. Oleksiuk, L. W. and Prenko, J. D., Bull. Am. Phys. Soc. II 7 (1962) 361.

4. H. E. Gove and A. E. Litherland, in Nuclear Spectroscopy, Part A, edited by Fag Ajzenberg-Selove (Academic Press, New York and London) (1960).

5. L. W. Fagg and S. S. Hanna, Rev. Modern Phys. 31 711 (1959).

6. P. Kossanyi-Demay, R. M. Lombard and G. R. Bishop, Nuclear Physics 62 (1965) 615.

7. A. E. Litherland, M. A. Clark and C. Broude, Phys. Letters 3 (1963) 204.

8. R. S. Blake, D. J. Jacobs, J. O. Newton and J. P. Schapira, Phys. Letters 14 (1965) 219.

9. R. Nordhagen, private communication.

10. G. I. Harris, H.J. Hennecke and F. W. Prosser, Jr., Phys. Letters 9 (1964) 324.

11. Yang Tan, Thesis, University of Kansas, (1964).

APPENDIX I

Analysis of Errors and the Least Squares Method

1. Introduction

The successful analysis of angular correlation data has depended quite heavily upon the least squares determination of parameters and upon the proper manipulation of errors including the effects of statistical correlations. Although much of this is well known it seems advisable to review in a general way the least squares and error analysis techniques which may be called upon implicitly or explicitly in the discussion of data analysis and in the actual analysis of data.

2. The Determination of Errors

2.1 Definition of Mean, Variance, Covariance, and Correlation

Let a series of R measurements of a quantity X_i yield the values $X_i(r)$, $r = 1, 2, \cdots, R$. The average value of X_i is

$$\overline{X_i} = [X_i]_{avg} \equiv \frac{1}{R} \sum_{r=1}^{R} X_i(r) \quad . \tag{1}$$

The variance of X_i is

$$var(X_i) \equiv \sigma_i^2 = [(X_i(r) - \overline{X_i})^2]_{avg} = \frac{1}{R} \sum_{r=1}^{R} (X_i(r) - \overline{X_i})^2 \quad , \tag{2}$$

The variance is the square of the standard deviation. In the event that several quantities $X_1, X_2, \cdots, X_i, \cdots$ are measured one can define the matrix

$$\sigma_{ij}^2 = [(X_i(r) - \overline{X_i})(X_j(r) - \overline{X_j})]_{avg} \quad . \tag{3}$$

The diagonal elements are the variances of the measured quantities and the off-diagonal elements are called the covariances:

$$\sigma_{ii}^2 \equiv var(x_i) \equiv \sigma_i^2$$

$$\sigma_{ij}^2 \equiv cov(x_i x_j) \quad for \quad i \neq j \quad .$$

The correlation factor between X_i and X_j can be defined by:

$$\sigma_{ij}^2 = \rho_{ij} \sigma_i \sigma_j \quad . \tag{4}$$

The correlation factor ρ_{ij} can be shown to take on values only between + 1 and -1. If X_i and X_j are statistically independent variables then $\rho_{ij} = 0$ so the variance-covariance matrix defined in (3) is diagonal. This matrix is also called the error matrix.

2.2 Errors in Functions of Several Measured Quantities

2.2.1 Linear Functions

Suppose the quantities $X_1, X_2, \cdots, X_n$ have been measured and the matrix σ_{ij}^2 is known.

IF $L(x_1, x_2, \cdots, x_n) = \sum_{i=1}^{n} l_i x_i$ then

$$var(L) = \sum_{ij} l_i l_j \sigma_{ij}^2 \quad . \tag{5}$$

As an example suppose n = 2 and $l_i = 1$. Then

$$var(x_1 + x_2) = \sigma_1^2 + \sigma_2^2 + 2\sigma_{12}^2 = \sigma_1^2 + \sigma_2^2 + 2\rho_{12}\sigma_1\sigma_2 \quad .$$

If $\rho_{12} = \rho_{21} = 0$ this reduces to the well known result that the variance of the sum is equal to the sum of the individual variances.

2.2.2 Non linear functions

If $F = \phi\ (X_1, X_2, \cdots, X_n)$ is nonlinear, the error in F can in many cases by approximated by

$$var(F) \simeq \sum_{i,j} \frac{\partial \phi}{\partial x_i} \frac{\partial \phi}{\partial x_j} \sigma_{ij}^2 \quad . \tag{6}$$

The approximation assumes that the probability distribution of $X_1, X_2, \cdots, X_n$ is concentrated in a relatively small region about $(\overline{X}_1, \overline{X}_2, \cdots, \overline{X}_n)$ and that F can be represented by the linear terms of Taylor series in the neighborhood about $(\overline{X}_1, \overline{X}_2, \cdots, \overline{X}_n)$.

One case of interest is the error in the ratio of two correlated quantities, say $\frac{X_1}{X_2} = R$.
Then we have

$$var(R) = R^2 \left\{ \frac{\sigma_1^2}{X_1^2} + \frac{\sigma_2^2}{X_2^2} - 2 \frac{\sigma_{12}^2}{X_1 X_2} \right\} \tag{7}$$

If $\rho_{12} = \rho_{21} = 0$ this reduces to the well known result that the fractional standard deviation of $\frac{X_1}{X_2}$ is the square root of the sum of fractional standard deviations of X_1 and of X_2.

3. The Least Squares Method

3.1 Uncorrelated Data

Suppose one has measured a number of quantities W_i, $i = 1, 2, \cdots, N$ and knows the variances σ_i^2. For example W_i might be the counting rate at angle θ_i and σ_i^2 determined by Poisson statistics. The functions $F_\ell(\theta_i)$ are known and the coefficients a_ℓ are desired in the expansion

$$W_i = \sum_{\ell=1}^{L} a_\ell F_\ell(\theta_i) \qquad i = 1, 2, \cdots, N \quad . \tag{8}$$

The best set a_ℓ will be that which minimize the value of $Q^2(a_\ell)$ where

$$Q^2 = \sum_{i=1}^{N} \omega_i \left(W_i - \sum_{\ell=1}^{L} a_\ell F_\ell(\theta_i) \right)^2 \quad . \tag{9}$$

ω_i is a statistical weight factor given by:

$$\omega_i = \frac{1}{var(W_i)} = \frac{1}{\sigma_i^2} \quad .$$

This assumes that the data is statistically uncorrelated as would be the case with a number of simple counting rate determinations. To minimize the function Q^2 with respect to the parameters a_ℓ, set $\frac{\partial Q^2}{\partial a_\ell} = 0$ for $\ell = 1, 2, \cdots, L$. This provides the L equations:

$$\sum_i \omega_i W_i F_\ell(\theta_i) = \sum_i \omega_i \sum_{\ell'} a_{\ell'} F_{\ell'}(\theta_i) F_\ell(\theta_i) \quad , \quad \ell = 1, 2, \cdots, L \, . \tag{10}$$

These equations are to be solved for a_ℓ. They are called the normal equations. Equations (10) are equivalent (after interchanging the order of the ℓ' and i summations) to the matrix equation

$$\vec{Y} = M \vec{a} \tag{11}$$

where $\vec{a}$ is a column vector with elements a_ℓ; $\vec{Y}$ is a column vector with elements $Y_\ell = \sum_i \omega_i W_i F_\ell(\theta_i)$; and M is a square L x L matrix with elements

$$M_{\ell\ell'} = \sum_i \omega_i F_\ell(\theta_i) F_{\ell'}(\theta_i) \quad .$$

Therefore the desired solution is

$$\vec{a} = M^{-1} \vec{Y} \quad . \tag{12}$$

The matrix M is called the normal matrix. It can be shown from the defining equation (3) that the elements of the inverse matrix M^{-1} are:

$$M^{-1}_{\ell\ell} \equiv var(a_\ell)$$
$$M^{-1}_{\ell\ell'} \equiv cov(a_\ell a_{\ell'}) \quad . \tag{13}$$

The inverse of the normal matrix is therefore the error or variance-covariance matrix and provides directly the desired errors in the expansion coefficients and their statistical correlations as well. As an example of the above it follows from equations (3) and (13) that the proper error in the ratio a_K/a_0 is:

$$var\left(\frac{a_K}{a_0}\right) = \left(\frac{a_K}{a_0}\right)^2 \left\{ \frac{M^{-1}_{KK}}{a_K^2} + \frac{M^{-1}_{00}}{a_0^2} - 2\,\frac{M^{-1}_{K0}}{a_K a_0} \right\} . \tag{14}$$

3.2 The Least Squares Fitting of Correlated Data

If the data W_i is correlated and the associated error matrix is known then a more general definition of Q^2 than that of eq. (9) is desired. The equation now becomes:

$$Q^2 = \sum_{i,j} \omega_{ij} \left[W_i - \sum_\ell a_\ell F_\ell(\theta_i)\right] \left[W_j - \sum_\ell a_\ell F_\ell(\theta_j)\right] . \tag{15}$$

The quantities ω_{ij} are the elements of the weight matrix which is the inverse of the error matrix belonging to the correlated data points ω_i. If the data is uncorrelated the error matrix is diagonal so the weight matrix is also diagonal and equation (15) becomes identical with equation (9). Equation (15) leads to the same solution:

$$\vec{a} = M^{-1}\,\vec{Y}$$

where now $(\vec{Y})_\ell = \sum_{ij} \omega_{ij}\, W_i\, F_\ell(\theta_j)$, and

$$M_{\ell\ell'} = \sum_{ij} \omega_{ij}\, F_\ell(\theta_i)\, F_{\ell'}(\theta_j) \quad .$$

3.3 Functions of More than One Independent Variable

It is desirable to apply the least squares method thus far developed to an expansion of the form

$$W(\theta_1, \theta_2, \phi) = \sum_{KMN} A^N_{KM}\, X^N_{KM}(\theta_1, \theta_2, \phi) \quad . \tag{16}$$

In order to do so one has only to replace

$$X^N_{KM}(\theta_1, \theta_2, \phi) \quad \text{by} \quad F_\ell(x_i), \qquad \text{where}$$

ℓ stands for a unique set KMN and X_i stands for the ith set of angles θ_1, θ_2, ϕ. Then one proceeds as before with

$$W_i = \sum_\ell A_\ell\, F_\ell(x_i) \quad . \tag{17}$$

One new and occasionally subtle feature is encountered in fitting functions of more than one independent variable. This feature is perhaps best illustrated by an example: Suppose 5 measurements are made at the points $\theta_1 = 90^\circ$, $\theta_2 = 90^\circ$, $\phi = 0^\circ, 30^\circ, 45^\circ, 60^\circ, 90^\circ$. We shall agree to call these 5 sets of angles X_1, X_2, X_3, X_4, X_5 in the order that they appear above. Suppose a fit with the 3 functions

X^{o}_{oo}, X^{o}_{20}, X^{o}_{02} is desired. That is, the best set of coefficients A^{N}_{KM} are required in the expansion

$$W_i = A^{o}_{oo} X^{o}_{oo}(x_i) + A^{o}_{20} X^{o}_{20}(x_i) + A^{o}_{02} X^{o}_{02}(x_i)$$

$$\equiv A_1 F_1(x_i) + A_2 F_2(x_i) + A_3 F_3(x_i) \quad .$$

This expansion defines the functions $F_\ell(X_i)$ mentioned in equation (17). However it is true that

$$F_2(x_i) = F_3(x_i) = 5/4\ F_1(x_i) \ , \quad i = 1, 2, \cdots, 5 . \tag{18}$$

Thus the functions are not linearly independent over the set $X_1, \cdots, X_5$ and no unique set of expansion coefficients can be found. This causes the normal matrix to be singular. Of course had a different set of angles which involved angles for θ_1 and θ_2 of other than 90^{o} been chosen, the functions F_1, F_2, F_3 would have been independent and the curve fit would be possible. There are less obvious possibilities. For example the five functions X^{o}_{oo}, X^{o}_{20}, X^{o}_{02}, X^{o}_{22}, X^{2}_{22} are not all linearly independent over the entire set of points spanned by the Ferguson-Rutledge geometries I, II, VI, and VII. It is necessary to include data from either an angular distribution or triple correlation data from a "non-standard" geometry in order to obtain a successful curve fit.

APPENDIX II

Computer Program for Angular Correlation Data Analysis

A program is described here which was used for the analysis of the $S^{34}(p,\gamma)Cl^{35}$ angular correlations. The general techniques which the program employs are described in Section 3. The program assumes that only one magnetic substate of the resonance level is populated. Modified versions of the program which allow the population of more than one magnetic substate are in use and all of the programs will be discussed in more detail elsewhere[1]. It would be simple enough to make one program to handle any number of magnetic substates but such a program would have resulted in a serious reduction in speed for the more simple problems.

The program consists of one executive control program and fifteen subroutines. The overall program logic is shown in figure 1. The function of the subroutines is discussed below.

1) READ - reads and stores all of the input data.

2) GRID - generates a set of angles running from -90° to $+90^{\circ}$ in equal increments of 2°, or greater, and calculates the tangents of these angles, δ_K, $K = 1, \cdots, N_g$. N_g is the total number of angles in the set.

3) ABCH - calculates the following functions:

$$A_{Mi} = \sum_{KN} E^{N}_{KM}(J_1 L_1 L_1 J_2)\, Q_K\, Q_M\, X^{N}_{KM}(\Omega_i)$$

$$B_{Mi} = \sum_{KN} E^{N}_{KM}(J_1 L_1 L'_1 J_2)\, Q_K\, Q_M\, X^{N}_{KM}(\Omega_i)$$

$$C_{Mi} = \sum_{KN} E^{N}_{KM}(J_1 L'_1 L'_1 J_2)\, Q_K\, Q_M\, X^{N}_{KM}(\Omega_i)$$

$$H_{Mk} = h_M(J_2 L_2 L_2 J_3) + \delta_K h_M(J_2 L_2 L'_2 J_3) + \delta_K^2 h_M(J_2 L'_2 L'_2 J_3)\,,$$

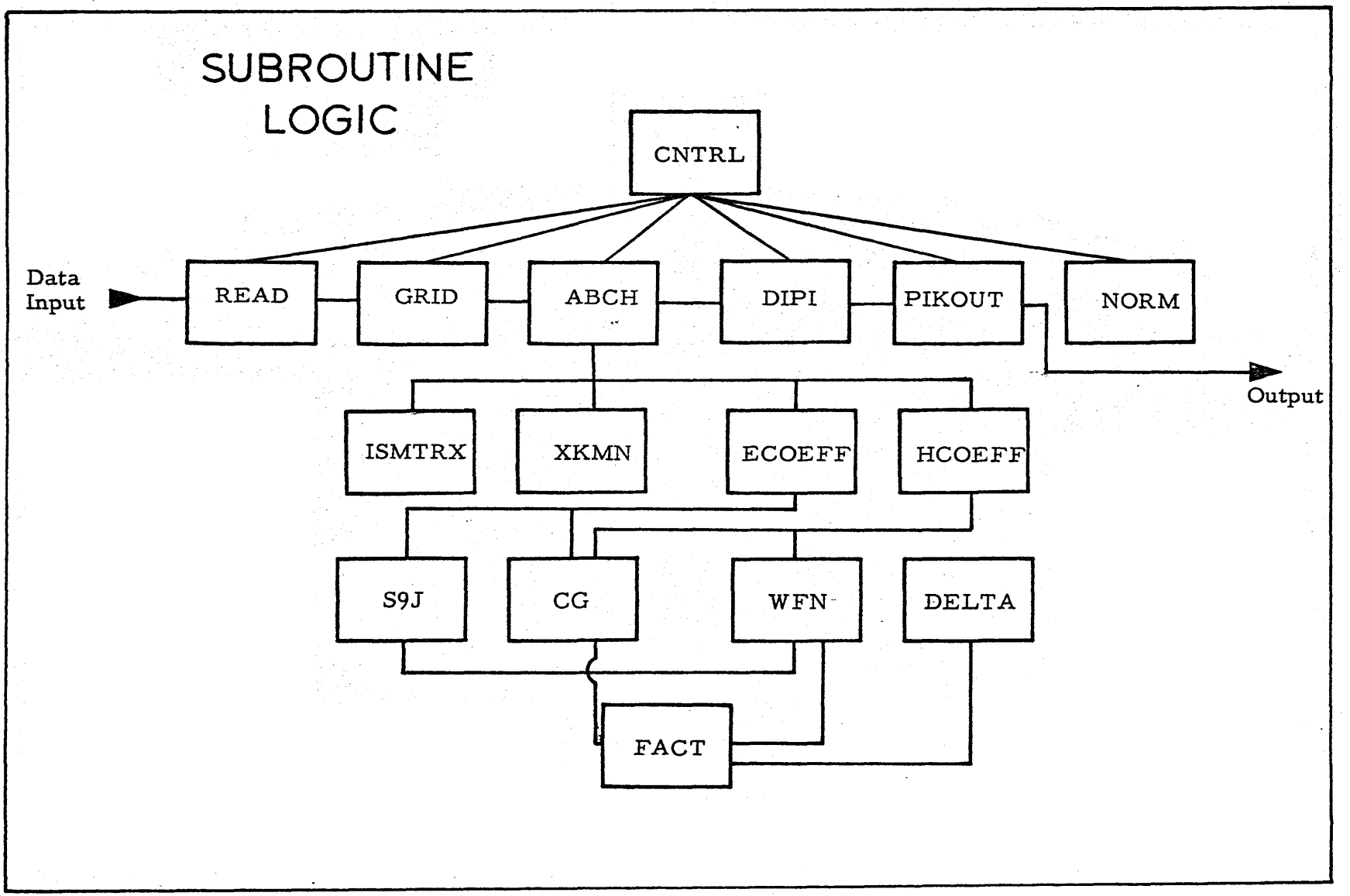
SUBROUTINE
LOGIC
CNTRL
Data
Input
READ
GRID
ABCH
DIPI
PIKOUT
NORM
Output
ISMTRX
XKMN
ECOEFF
HCOEFF
S9J
CG
WFN
DELTA
FACT

Fig. 1

where Ω_i is the ith set of experimental points and i runs over the entire set of points.

4) DIP1 - calculates the valve of chi-squared for each point of an $N_g \times N_g$ grid. The theoretical value at the k, ℓ grid point is now given by the simple expression

$$W_{Th}(\Omega_i) = P_1 \sum_M (A_{Mi} + \delta_k B_{Mi} + \delta_k^2 C_{Mi}) H_{M\ell} \quad .$$

The single population parameter is obtained by least squares analysis as:

$$P_1 = \frac{\sum_i \omega_i W_{exp}(\Omega_i) W_{Th}(\Omega_i)}{\sum_i \omega_i [W_{Th}(\Omega_i)]^2} \quad .$$

5) PIKOUT - scans the chi-squared surface to produce the "shadow" lines and recalls DIP1 to obtain the values of the theoretical points at the absolute minimum point in the chi-squared surface. The results are then written on the output device.

6) NORM - renormalizes the experimental input data, if necessary, and branches back to DIP1 to calculate a new chi-squared surface.

7) ISMTRX - generates the maximum values of the K, M and L indices subject to the various triangle conditions for the particular spin sequence under consideration and generates an index suppression scheme to suppress K, M, N into a single running index.

8) XKMN - calculates the functions $X^N_{KM}(\theta_1, \theta_2, \phi)$.

9) ECOEFF - calculates $E^N_{KM}(J_1 L_1 L_1' J_2)$ coefficients

10) HCOEFF - calculates $h_M(J_2 L_2 L_2' J_3)$ coefficients

11) S9J - calculates the 9-J symbols necessary for the E^N_{KM} coefficients.

12) CG - calculates Clebsch-Gordon coefficients.

13) WFN - calculates Racah coefficients.

14) DELTA - calculates triangle coefficients which are necessary for WFN.

15) FACT - is a factorial table.

The arrays A_{Mi}, B_{Mi}, C_{Mi}, and H_{MK} are calculated and stored by the subroutine ABCH in order to prevent redundant arithmetic operations in the calculation of the theoretical values at each grid point. For a grid of 2^o intervals and for 50 data points, the computer must calculate over 400,000 theoretical values. It is, therefore, crucial that each theoretical value be calculated with as few operations as possible.

The input to the program is indicated below:

Card Numbers	Columns	Input
1	1-48	Identification
2	1-3	Geometry Label (optional)
	4-5	Number of data cards in this geometry = N_1
	6-10	Q_M M = 0
	16-20	Q_K K = 0
	26-30	Q_M M = 2
	36-40	Q_K K = 2
	46-50	Q_M M = 4
	46-60	Q_K K = 4

Card Numbers	Columns	Input	
	66-70	Q_M M = 6	
	76-80	Q_K K = 6	
3-(N_1 + 3)	1-10	θ_1	
	11-20	θ_2	
	21-30	ϕ	
	31-40	Experimental value at θ_1, θ_2, ϕ	
	41-50	Standard deviation	
(N_1 + 3)-N_f	The card sequence 2-(N_1 + 3) may be repeated to include angular distribution data and/or separate triple correlation geometries. Each such set of data will be separately normalized by the normalization routine.		
N_f + 1	1-3	The word END must be present to indicate that all of the data has been entered.	
N_f + 2 (integer spins)	10	J1	1st spin sequence
	20	J2	to be tried
	30	J3	
	35-40	Grid intervals in degrees	
	50-58	The word NORMALIZE will cause various geometries to be normalized with respect to each other	
or			
N_f + 2 (half integer spins)	10-12	J1/2	1st spin sequence
	20-22	J2/2	to be tried
	30-32	J3/2	
	35-40	same as above	
	50-58	same as above	

Additional spin sequences may follow.

The output from the program is as follows:

1. The experimental values used in the calculation and the theoretical values corresponding to the lowest point in the chi-squared surface.
2. If 5^{o} intervals are used in arctan δ, a solid block of three digit fixed point numbers is generated. These numbers are the truncated values of chi-squared over the entire surface. This output is suppressed if intervals of other than 5^{o} are used.
3. Finally, the projections of the chi-squared surface onto the δ_1 plane and the δ_2 plane are listed.

All of the output is labelled and each page is headed by the identifying information contained on the first input card.

References to Appendix II

1. Hyder and Watson, ARL Technical Documentary, (to be published).

ACKNOWLEDGEMENTS

The work described in this dissertation is a part of a program for the investigation of properties of light nuclei which is supported in part by the Atomic Energy Commission under the project direction of Dr. R. W. Krone, Dr. F. W. Prosser, and Dr. L. W. Seagondollar. Dr. Seagondollar has served as my advisor throughout my entire graduate career. His assistance, direction, and understanding are sincerely appreciated. The assistance and advice of Dr. F. W. Prosser and Dr. R. W. Krone are also gratefully acknowledged.

The latter portion of this work was completed during my employment at the Aerospace Research Laboratories at W.P.A.F.B., Ohio. The aid and cooperation of the ARL administrative staff and support organizations have been exceptional and are greatly appreciated.

Dr. G. I. Harris has been associated with all phases of this work and his advice, leadership, and collaboration have been a great influence. The consultation of Dr. H. J. Hennecke has also been valuable.

Many other people have contributed to this work. Some of them are mentioned below:

F. D. Lee, who collaborated with me during the early part of this work, and who has contributed far more than he has accepted credit for.

A. K. Hyder, for his untiring efforts in helping with some of the experiments, programming the computer, and drawing the figures for the thesis.

This work, as well as my entire graduate and undgraduate

education, has been made possible by the understanding and selfless support of my wife, Joyce.